

Article

Key Structure Design and Experiment of Air-Suction Vegetable Seed-Metering Device

Jian Xu , Junwei Hou , Weibin Wu ^{*}, Chongyang Han, Xiaoming Wang, Ting Tang and Shunli Sun

College of Engineering, South China Agricultural University, Guangzhou 510642, China; xujianaa@stu.scau.edu.cn (J.X.); junweihou@scau.edu.cn (J.H.); 20202009003@stu.scau.edu.cn (C.H.); ebianwxm1234@stu.scau.edu.cn (X.W.); 20203163056@stu.scau.edu.cn (T.T.); sunshunli@stu.scau.edu.cn (S.S.)
^{*} Correspondence: wuweibin@scau.edu.cn

Abstract: The air-suction precision seed-metering device is prone to the instability of the seed adsorption state, which arises from blockage of the suction hole and leads to uneven seeding. This paper analyzed and determined key structural parameters of the seed-metering plate, then established an adsorption mechanics model of the seed during the migration process and designed the key structure of the air-suction seed-metering device with the aim of improving the uniformity of high-speed direct seeding of vegetables. Furthermore, we used the DEM-CFD coupling method to analyze the influence of the law of seeds on the change of the flow field with different hole types. Results showed that the turbulent kinetic energy ($202.65 \text{ m}^2 \cdot \text{s}^{-2}$) and the coupling force to the seeds (0.029 N) of the B-type hole are the largest, which is the best fluid domain structure for the suction hole of the seed-metering plate. Moreover, we used Adams to analyze the meshing process between the knock-out wheel and the seed-metering plate, affirming the rationality of the knock-out wheel design. Finally, in order to improve the working efficiency of the seed-metering device, we performed one-factor and response surface experiments of seeding performance using the air-suction seed-metering device designed with the optimized structure as the experimental object. Analysis of the influence of weights across each factor on the experimental performance evaluation indicators revealed an optimal combination of seeding performance parameters in the air-suction seed-metering device, namely a seed-throwing angle of 13° , a working speed of 14.5 km/h , and negative pressure of 3.1 kPa . Results from verification experiments revealed the corresponding experimental indicators, namely qualified, multiple, and missing indexes of 95.9 , 1.2% , and 2.9% , respectively.

Keywords: seed-metering device; DEM-CFD coupling; knock-out wheel; seeding uniformity



Citation: Xu, J.; Hou, J.; Wu, W.; Han, C.; Wang, X.; Tang, T.; Sun, S. Key Structure Design and Experiment of Air-Suction Vegetable Seed-Metering Device. *Agronomy* **2022**, *12*, 675. <https://doi.org/10.3390/agronomy12030675>

Academic Editor: Simon Pearson

Received: 19 January 2022

Accepted: 8 March 2022

Published: 11 March 2022

Publisher's Note: MDPI stays neutral with regard to jurisdictional claims in published maps and institutional affiliations.



Copyright: © 2022 by the authors. Licensee MDPI, Basel, Switzerland. This article is an open access article distributed under the terms and conditions of the Creative Commons Attribution (CC BY) license (<https://creativecommons.org/licenses/by/4.0/>).

1. Introduction

Precision seeding technology, which takes into account the seeding rate, seed spacing, and seeding depth as the core control objectives, is the main mode of modern standardized operation of vegetables. The technology, which plays an important role in reducing the operating frequency of seeding equipment, as well as improving seeding quality and economic benefits, is one of the main modes of production for large-scale planting of vegetable crops in developed countries [1–3]. However, during the large-scale precision planting of vegetables, the suction holes of the seed-metering device in the planter are prone to clogging, a phenomenon that causes an issue with uneven seed flow. This subsequently causes severe damage to the good growth environment of seeds and restricts vigorous promotion and application of precision seeding technology. To solve these problems, researchers have attempted to optimize the design of precision seeding-metering devices [4,5].

For example, Maleki et al. designed a compound screw device based on the internal structure of the mechanical seed-metering device, which ameliorated the irregular phenomenon caused by fluctuation of the seed stream and blockage of holes and enhanced the seeding uniformity of mechanical seeders [6]. On the other hand, Chen et al. designed

a type of an inlaid, combined, mechanical seed-metering device. Particularly, the inlay blocks comprising different holes arranged in double or single rows coupled with primary and auxiliary slot plates effectively resolved the challenge of the high seed-breakage rate [7]. In a departure from traditional optimization design methods, some researchers have attempted to apply neural network calculation models for the optimization of seed-metering devices. For instance, Ananthacha et al. proposed the use of an artificial neural network to predict seed-metering performance parameters of the sloping disc seed-metering device. Particularly, a genetic algorithm was used as a single-objective constraint optimization tool for the determination of the optimal structure of the neural network model, thereby improving the seed-unloading uniformity of the seed-metering device [8]. Overall, the above studies mainly aimed at enhancing the mechanical precision of the seed-metering device. These studies have improved the issue of seed damage and blockage of the suction hole resulting from the too-small suction hole of the seeding device to a certain extent. However, the sharp decline in seeding quality persists in cases where the mechanical seed-metering device has a high operating speed and a faster seeding frequency. To date, the development of the mechanical seed-metering device is still constrained by technical bottlenecks.

The air-suction seed-metering device is one form of pneumatic seed-metering device, which mainly works on the principle of the adsorption, transportation, and delivery of seeds through airflow. The device is in contact with seeds through airflow, which ensures adaptation to the seed shape and reduces damage. Currently, this is the most widely applied seed-metering device. However, the problem of uneven seed flow in the air-suction seed-metering device has not been effectively solved in the case of a high seeding frequency [9–11]. To solve this problem, Shi et al. designed the curve-shaped hole guide groove to separate seeds from the seed tray according to the established trajectory under the action of the seed pusher [12]. On the other hand, Yang et al. developed an arc-shaped seed unloader and applied the principle of relative motion to sequentially pull out the seeds from the seed tray socket [13]. Moreover, Ding et al. analyzed the seed unloading process of the air-suction seed-metering device and concluded that under high-speed planting operations, the seed-unloading mechanism has a greater impact and vibration on the seed-metering plate, which easily causes absorption of the seeds into the suction hole, thereby causing them to prematurely fall. In addition, the suction hole, under continuous seeding operation, is easily blocked by broken seeds and impurities, causing missed seeding and seriously affecting the quality of seeding operations [14].

This article focuses on the existing air-suction seed-metering device. This device easily causes instability of the seed adsorption state due to clogging of the suction hole, which leads to uneven seeding. According to the adsorption mechanics model of the seed during the migration process, we designed the key structure of the air-suction seed-metering device. We used the DEM-CFD coupling method to analyze the influence of the law of seeds on the change of flow field and used Adams to perform a kinematics analysis of the meshing process between the knock-out wheel and seed-metering plate. The main factors affecting the seed-metering performance were analyzed, and the three-factor quadratic rotation orthogonal combination test of the seed-metering device revealed an optimal combination of seeding performance parameters in the air-suction seed-metering device.

2. Materials and Methods

2.1. Structure and Working Principle of the Seed-Metering Device

The air-suction, high-speed, precision seed-metering device mainly comprises a seed-metering plate, a seed-cleaning mechanism, an air chamber shell, a seed-unloading mechanism, a transmission shaft, a sealing air cushion, and other components. A profile of this device is shown in Figure 1. For effective working of the seed-metering device, there is a need to first install a seed-metering plate, followed by sequential installation of seed-cleaning and seed-unloading mechanisms inside the seed-metering device. Next, a seed cleaning knife is adjusted to a reasonable position, then the rear plate surface of the seed-metering plate is closely fitted with the sealing air cushion. Thereafter, the variable-frequency vac-

uum pump is connected to the air inlet to allow the air chamber shell, sealing air cushion, and seed-metering plate to form a negative-pressure chamber. When the seed-metering device starts working, the seeds enter the seed-filling chamber from the seed inlet, while the motor drives the seed-metering plate to rotate through the transmission shaft. The entire working process can be divided into several areas, namely seed-filling, transition, seed-clearing, seed-carrying, and seed-unloading areas, as shown in Figure 2.

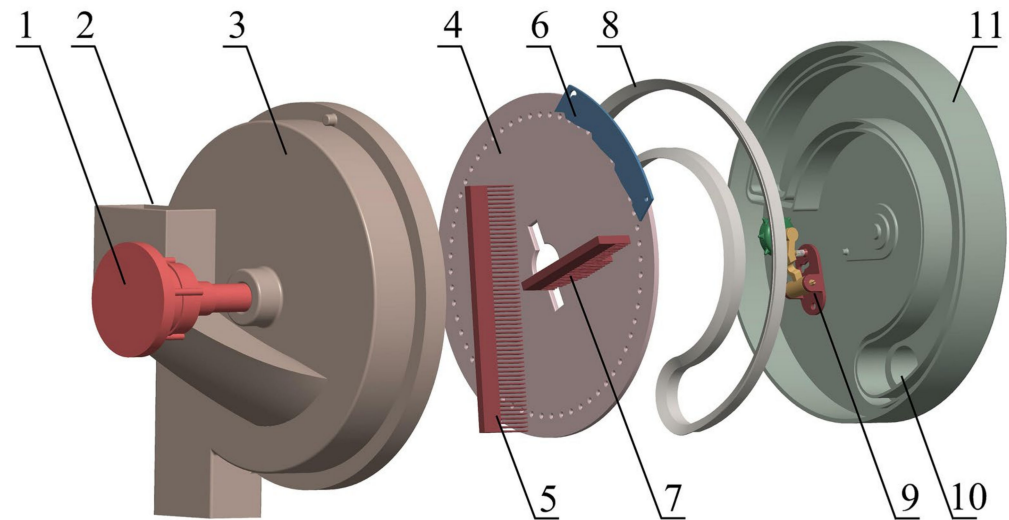


Figure 1. Profile of the structure of the air-suction seed-metering device: (1) Transmission shaft; (2) seed inlet; (3) seed-metering device main shell; (4) seed-metering plate; (5) seed-blocking brush; (6) seed-cleaning knife; (7) impurity-removal brush; (8) sealing air cushion; (9) seed-unloading mechanism; (10) suction inlet; (11) air-chamber shell.

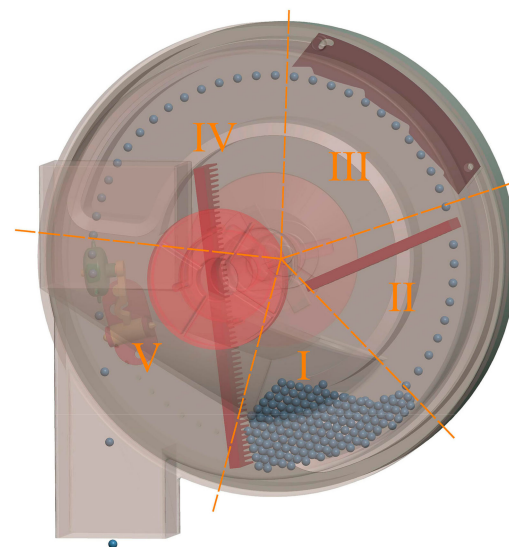


Figure 2. Schematic representation of working area division of the seed-metering device: (I) seed-filling area; (II) transition area; (III) seed-clearing area; (IV) seed-carrying area; (V) seed-unloading area.

When the seed-metering device is working normally, seeds fall into the seed-filling area under the action of gravity, and the negative pressure airflow passes through the suction holes on the seed-metering plate to adsorb the seeds into the seed-filling area. Single or multiple seeds, stably adsorbed into the suction hole, undergo circumferential rotation under the action of the transmission shaft until they cross the transition area and enter the seed-clearing area. Excess seeds in the suction hole of the seed-clearing area

collide with the teeth of the seed-cleaning knife and fall back to the seed-filling area under the knife's action. Subsequently, single seeds that are stably adsorbed onto the suction hole continue to rotate in a circumferential direction with the seed-metering plate until they enter the seed-unloading area from the seed-carrying area. The negative-pressure airflow in the seed-unloading area disappears, causing the seeds to fall under pressure from gravity and centrifugal force. At the same time, the seed-unloading mechanism located on the rear surface of the seed-metering device further blocks the negative pressure airflow, thereby removing potential impurities to ensure uniform delivery of seeds for precision seeding.

2.2. Key Parameter Design of Seed-Metering Plate

2.2.1. Determination of Seed-Metering Plate Diameter

The seed-metering plate is a key component for realizing high-speed and precise seeding. Particularly, its diameter is very important for the suction hole number, adsorption pressure, and the design of the seed-unloading mechanism of the seed-metering device [15,16]. According to the relationship between the rotation speed of the seed-metering plate and the seed-filling time:

$$\begin{cases} t = \frac{L}{v_u} \\ L_a = \alpha \left(\frac{D_u}{2} - R_b \right) \\ v_u = \frac{\pi n_u}{30} \left(\frac{D_u}{2} - R_b \right) \end{cases} \quad (1)$$

where t is the time (s) the suction hole takes to stay in the seed-filling area; L is the arc length (m) of the seed-filling area; v_u is the linear velocity (m/s) of the seed-metering plate; α is the seed-filling angle (rad); D_u is the diameter (m) of the seed-metering plate; n_u is the rotation speed (r/min) of the seed-metering plate; while R_b is the radial distance (m) between the center of the suction hole and the edge of the seed-metering plate.

It can be obtained using Equation (1):

$$t = \frac{30\alpha}{\pi n_u} \quad (2)$$

According to Equation (2), the seed-filling time t is only related to the seed-filling angle α and the rotating speed n_u of the seed-metering plate. Therefore, increasing the diameter of the seed-metering plate cannot prolong the residence time of the suction hole in the seed-filling area. That is, the diameter of the seed-metering plate has nothing to do with the seed-filling performance. The radius of the seed-metering plate of the existing pneumatic seed-metering device is generally 80–260 mm. Since the seeding object of the seed-metering device designed in this paper is pelletized vegetable seeds, the seeding frequency is relatively high under the requirements of agronomy. In order to take into account the overall structure design of the seed-metering device, we selected a diameter of 240 mm, a thickness of 4 mm, and a radial distance of 15 mm between the center of the suction hole and the edge of the seed-metering plate.

2.2.2. Determination of Suction Holes

Based on the agronomic requirements of high-speed and precision direct seeding of field vegetables, we designed a seed-metering plate with a rotation speed of $n_u \leq 100$ r/min and a forward speed of the planter of $v_e \leq 18$ km/h. According to the relationship between the frequency of seeding and the plant spacing:

$$\begin{cases} f_k = \frac{v_u}{\delta_L} = \frac{v_e}{d} \\ k \cdot \delta_L = 2\pi \left(\frac{D_u}{2} - R_b \right) \\ v_u = \frac{\pi n_u}{30} \left(\frac{D_u}{2} - R_b \right) \end{cases} \quad (3)$$

where f_k is the seeding frequency (1/s); v_e is the forward speed (m/s) of the planter; δ_L is the distance (m) between adjacent suction holes; d is the plant spacing (m), whereby the reasonable plant spacing of field vegetables is 0.05–0.3 m; while k is the number of suction holes in the seed-metering plate.

From Equation (3), $10 \leq k \leq 60$. Simultaneously, Equations (2) and (3) can obtain:

$$t = \frac{k \cdot \alpha}{2\pi f_k} \quad (4)$$

According to Equation (4), the seed-filling time t is proportional to the number of suction holes k . Under fixed conditions of the plant spacing and seed-metering plate diameter, an increase in the number of suction holes causes the plate to absorb relatively more seeds, which is beneficial to reducing the plate's rotation speed required for actual seeding. The maximum working speed of the designed seed-metering device is 18 km/h. When the plant spacing is 0.15 m, if the number of suction holes $k = 40$, then $n_u = 50$ r/min; if the number of suction holes $k = 60$, then $n_u = 33.3$ r/min, whereby the relative speed of the seed-metering plate is reduced by 33% at this time. Therefore, the central angles of adjacent suction holes are set as integers in order to improve the seeding efficiency and ensure processing accuracy requirements. In this paper, the number of suction holes and the center angle of adjacent suction holes are set to $k = 60$ and 6° , respectively.

2.2.3. Determination of Suction Hole Diameter

When the suction hole is transferred to the seed-filling area, the airflow generated by the vacuum pump captures the seeds through the suction hole and maintains a stable adsorption state. On the other hand, when the seeds are transferred to the seed-unloading area, the seed-unloading mechanism performs auxiliary seeding on the seeds via relative rotation with the suction hole. Therefore, the size of the suction hole is a key aspect for effective stable capture of seeds and the design of the seed-unloading mechanism. Taking a single seed to be adsorbed by the suction hole as the research object, and assuming that the seed is a rigid body with uniform material, without considering other factors such as vibration and collision between seeds, the force analysis of the seed in the adsorption state is shown in Figure 3. According to the theory of rigid body dynamics, a force equation of the seed is established as follows:

$$\left\{ \begin{array}{l} F_Q = G + F_n + F_f \\ (F_s - N_Q) \cdot \frac{D_i}{2} = F_Q \cdot H \\ J = \sqrt{G^2 + F_n^2 + 2G \cdot F_n \cos \varphi_1} \\ K = \sqrt{J^2 + F_f^2 + 2J \cdot F_f \cos \varphi_2} \\ N_Q = N_a + N_b \\ F_n = m\omega^2 R_a \\ S = \frac{\pi D_i^2}{4} \\ P_0 = \frac{F_s}{S} \end{array} \right. \quad (5)$$

where G is the seed gravity, N; F_n is the centrifugal force, N; F_f is the friction force, N; F_Q is the vector resultant force of G , F_n , and F_f , N; D_i is the diameter of the suction hole, m; F_s is the adsorption capacity of the suction hole to the seed, N; N_Q is the side vector resultant force, N; N_a and N_b are support forces of the side wall of the suction hole on the seed, N; J is the resultant force of G and F_n , N; K is the resultant force of J and F_f , N; P_0 is the pressure difference between the two sides of the suction hole, Pa; φ_1 is the angle between G and F_n , ($^\circ$); ω is the angular velocity of the seed-metering plate, rad/s; φ_2 is the angle between J and F_f , ($^\circ$); S is the cross-sectional area of the suction hole, m^2 ; H is the distance

between the seed centroid and the seed-metering plate, m ; and R_a is the radius of the hole distribution circle, m .

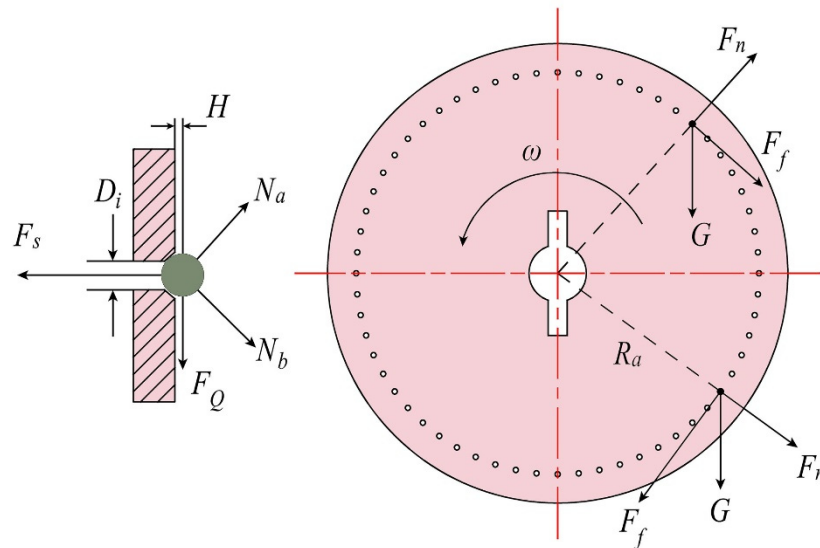


Figure 3. Force analysis diagram of seed adsorption state.

According to Equation (5), while considering the influence of its own conditions and objective conditions in the actual work of the seed-metering device, the adsorption pressure required at the moment when a single seed is captured by the suction hole can be obtained as:

$$P_0 = \frac{8HK_1K_2}{\pi D_i^3} \sqrt{G^2 + F_n^2 + 2GF_n \cos \varphi_1 + 2\sqrt{G^2 + F_n^2 + 2GF_n \cos \varphi_1} \cdot F_f \cos \varphi_2 + F_f^2} \quad (6)$$

where K_1 is the reliability coefficient of seed absorption, ranging from 1.8–2.0, while K_2 is the working reliability coefficient, ranging from 1.6–2.0. According to Formula (6), when $\cos \varphi_1 = \cos \varphi_2 = 1$, the maximum adsorption pressure required to capture seeds at the moment of the suction hole can be determined as follows:

$$P_{0\max} = \frac{8K_1K_2Hmg}{\pi D_i^3} \left(1 + \lambda + \frac{\omega^2}{g} R_a \right) \quad (7)$$

where $P_{0\max}$ is the maximum critical adsorption pressure, Pa, while λ is the comprehensive friction coefficient of the seed. Among $\lambda = (6 \sim 10) \tan \zeta$, ζ is the natural angle of repose of the seed.

According to the suction hole diameter formula [17], $D_i = (0.64 \sim 0.66)\bar{d}$, where \bar{d} is the average seed diameter (mm). In this paper, we selected pelletized vegetable seeds, with an average particle size of (4.0–4.2) mm and a calculated suction hole diameter range of (2.6–2.8) mm, as the planting objects. From Formula (7), it can be seen that the adsorption pressure is inversely proportional to the 3rd power of the suction hole diameter and proportional to the 2nd power of the rotation speed. If the diameter of the suction hole is smaller, the adsorption pressure required to capture the seed is larger. Therefore, in this paper, it is determined that the suction hole has a diameter of 2.8 mm.

2.3. Design of Seed-Unloading Mechanism

2.3.1. Installation Angle of Seed-Unloading Mechanism

The seed-unloading process is the last link in the working of the seed-metering device. The installation position of the seed-unloading mechanism directly affects the uniformity of seed flow [18,19]. Previous evidence has shown that most of the seeds are discharged along the tangential direction of the suction hole distribution circle at the same point in the seed-unloading area of the seed-metering device [20].

Seed motion after separation from the suction hole is illustrated in Figure 4. Assuming that the seed separation from the suction hole is O_1 and the speed of the seed is v_0 , the motion equation after the seed leaves the suction hole is as follows:

$$\begin{cases} v_x = v_u - R_a \omega \sin \beta \\ v_y = R_a \omega \cos \beta + gt_0 \end{cases} \quad (8)$$

$$\beta = \frac{2\pi n_u t}{60} \quad (9)$$

where v_x is the horizontal velocity of the seed, m/s; v_y is the vertical velocity of the seed, m/s; β is the seed-throwing angle, ($^\circ$); and t_0 is the elapsed time after the seed is separated from the seed-metering plate, s.

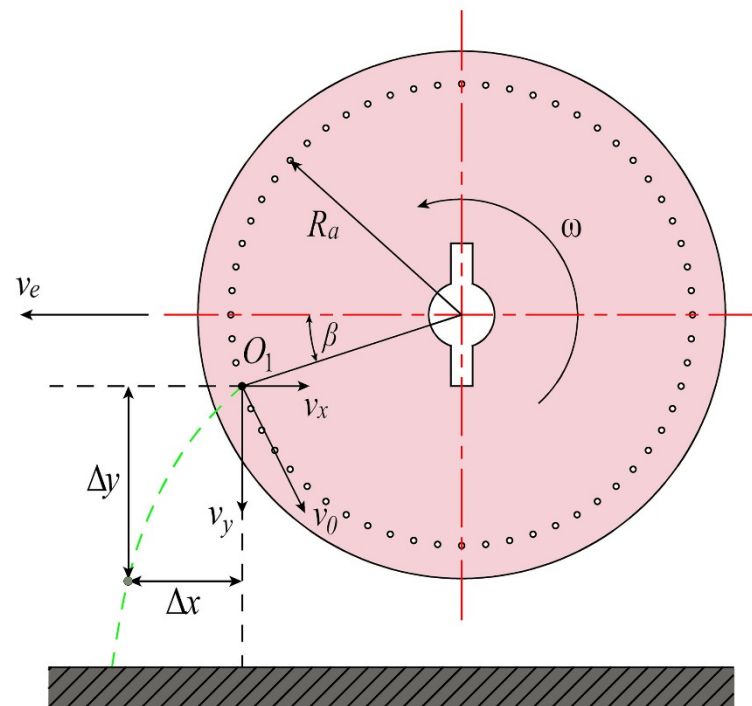


Figure 4. Diagrammatic representation of seed motion after separation from the suction hole.

Zero-speed seeding, that is, a horizontal speed when the seed falls, is equal to the forward speed of the planter, but in the opposite direction. At this time, the seed-unloading process of the seed-metering device can reduce the redundant bounce of the seed and uneven seeding. When zero-speed seeding is adopted, that is, $v_u = R_a \omega \sin \beta$, this indicates that the trajectory of the seed separated from the suction hole is related to the radius, the rotation speed of the seed-metering plate, and the seed-throwing angle. According to the seed-metering plate radius, determined in Section 2.2.1, it is evident that the rotation speed and seed-throwing angle will directly affect the seeding performance of the seed-metering device. In addition, a higher rotation speed generates greater vibration, which is likely to cause separation of the seeds adsorbed at the end of the seed-carrying area from the suction hole in advance, thereby resulting in an uneven seed flow due to the different positions of the seed-unloading points. In order to ensure that the seed-metering device has a good adsorption effect on the seeds in the seed-carrying area, it is important to not only prevent seeds from prematurely leaving the suction hole, but also reduce seed bouncing. Results from preliminary experiments indicate that the seed-throwing angle is $0^\circ \sim 30^\circ$. At the same time, we add a seed-unloading mechanism with anti-clogging and seeding uniformity-enhancing characteristics in order to prevent impurities and airflow from interfering with the seeding process.

2.3.2. Meshing Frequency and Base Circle Design of Knock-Out Wheel

The seed-unloading mechanism, which is located on the rear surface of the seed-metering plate, is mainly composed of a knock-out wheel alongside its supporting mechanism. When the seed-unloading mechanism is working, the knock-out wheel is driven by the rotation of the seed-metering plate, and each tooth of the knock-out wheel meshes with the suction hole. Notably, its working speed can reach 18 km/h, owing to the high speed of the designed seed-metering device, which requires a high meshing performance between the knock-out wheel and the seed-metering plate. There is a need to avoid interference between the knock-out wheel teeth and the suction hole of the seed-metering plate, which can cause instability of the meshing transmission. Therefore, reasonably designing the meshing frequency of the knock-out wheel and the seed-metering plate is imperative to making the meshing stable and reliable. The meshing relationship between the knock-out wheel and the seed-metering plate is shown in Figure 5. To smoothen the mesh, the distance between the teeth of the knock-out wheel in the circumferential direction is made consistent with that of the suction holes of the seed-metering plate in the circumferential direction. This is obtained as follows:

$$\frac{2\pi R_a}{k} = \frac{2\pi r_a}{z} \quad (10)$$

where r_a is the base circle radius (mm) of the knock-out wheel, while z is the number of knock-out wheel teeth.

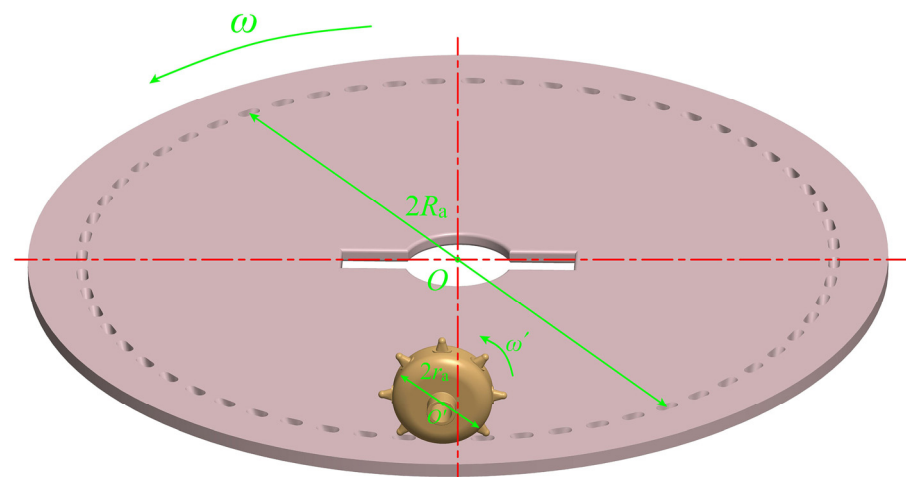


Figure 5. The meshing relationship between knock-out wheel and seed-metering plate.

The radius of the seed-metering plate and the number of suction holes have been determined in Section 2.2. Substituting them into the above formula results in $r_a = 1.75z$. Taking into account the installation position of the knock-out wheel and the size of the air chamber, we select 8 and 14 mm as the number of teeth z and the base circle radius r_a of the knock-out wheel, respectively. When the working speed is 18 km/h and the plant spacing is 25 cm, the meshing frequency between the knock-out wheel and the suction hole of the seed-metering plate is 20 Hz, the period is 0.05 s, whereas the rotation frequency of the knock-out wheel tooth is 2.5 Hz.

2.4. Two-Phase Flow Coupled Analysis of Seeds Adsorbed on Suction Holes

The traditional suction holes in the form of straight holes cannot meet the geometric requirements of the meshing of the knock-out wheel and the suction holes of the seed-metering plate. According to the geometric conditions of their meshing motion, three different suction hole structures A, B, and C are designed as shown in Figure 6. In the process of seed adsorption by the suction hole of the seed-metering plate, the airflow will have an adsorption effect on the seeds, and the seeds will also affect the change of the flow field of the suction hole. The two-phase flow coupling information of the suction fluid

domain was analyzed by the discrete element method and computational fluid dynamic (DEM-CFD) coupling method to obtain the optimal suction hole structure.

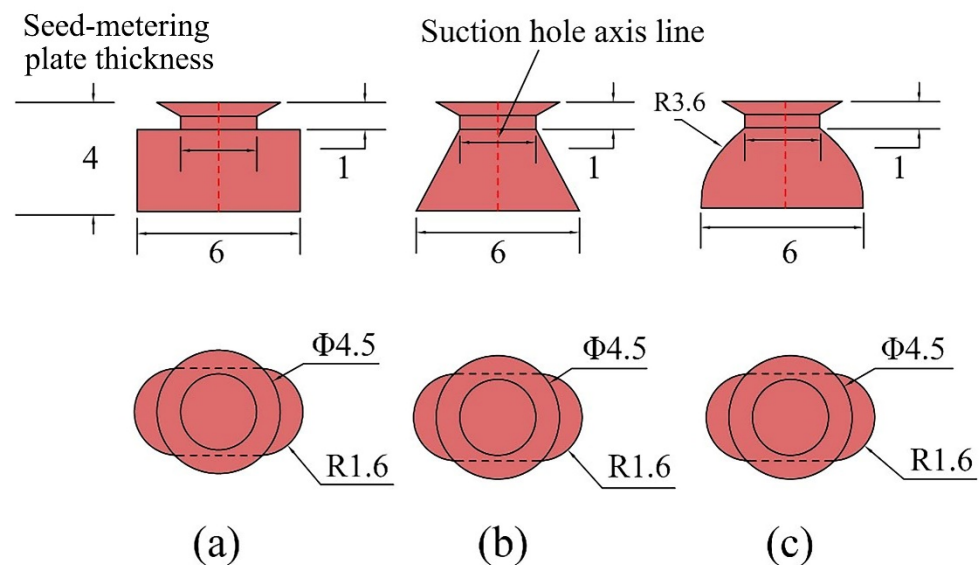


Figure 6. Geometric information of three suction holes (a–c).

The fluid domain with relatively large flow velocity needs to be finely meshed in the suction hole structure. However, the existing EDEM-Fluent coupling model cannot accurately analyze the situation that the particle volume is larger than the mesh volume in the fluid domain. This paper established a particle model of the pelleted vegetable seeds using the bonded-particle model method to solve the problem of CFD-DEM coupling accuracy, as shown in Figure 7. The bonded-particles model represents the whole particle as a polymer with a specific number of sub-particles, where the sub-particles are bonded with cohesive bonds. The sub-particle size is smaller than the minimum mesh size of the suction hole, and the dynamic behavior of the whole particle is determined based on the motion of each sub-particle and the forces and moments acting between the sub-particles. The calculation time of CFD and DEM were set at 5×10^{-4} s and 1×10^{-6} s, respectively. The input parameters used in the simulation were determined using pre-experiments (Table 1).

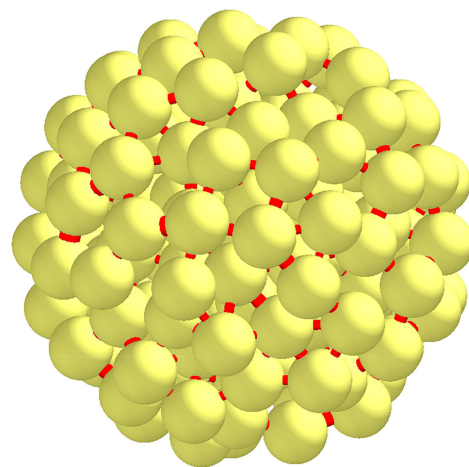


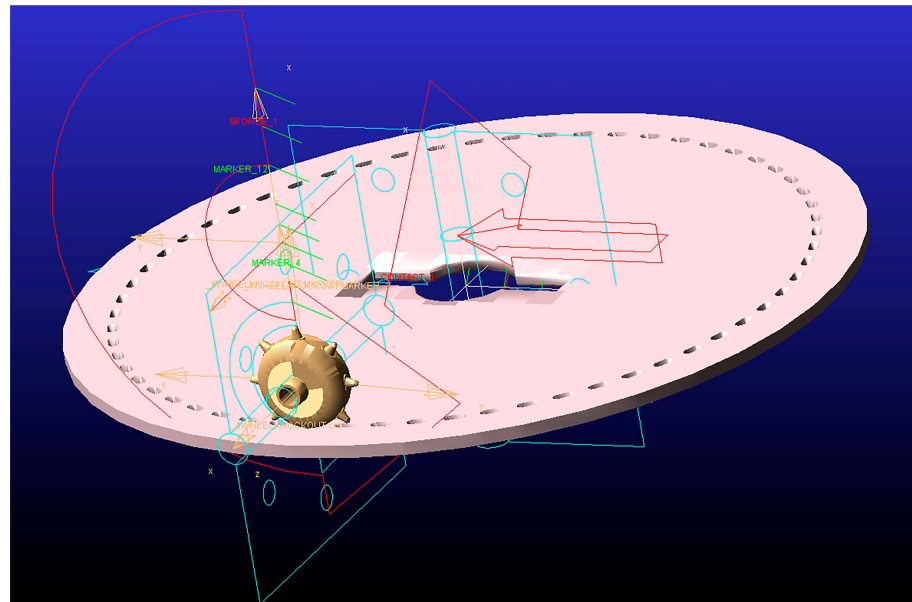
Figure 7. Seed bonded-particle model.

Table 1. DEM-CFD coupling simulation parameters.

Parameters	Symbols	Particle	Suction Hole Material
Density, kg/m ³	ρ	1340	1800
Poisson's ratio	ν	0.4	0.35
Shear modulus, Pa	G	1.50×10^8	1.30×10^9
Coefficient of restitution	e	0.526	0.627
Coefficient of static friction	μ	0.297	0.41
Coefficient of rolling friction	μ_r	0.03	0.026

2.5. Analysis of Meshing Motion Characteristics between Knock-Out Wheel and Seed-Metering Plate

In a high-speed seed-metering device, the force in the meshing process between the seed-metering plate and the knock-out wheel is very complicated. In this paper, we sought to further verify the rationality of the designed knock-out wheel tooth profile and analyze the overall reliability and stability of the meshing process. Specifically, we established a parameterized model of the knock-out wheel and seed-metering plate using the automatic mechanical system analysis software Adams, then performed dynamic analysis of the meshing process. Constraints and driving conditions were added to the parameterized model in Adams software, as shown in Figure 8. Next, we applied a load torque of 20 N·mm to the knock-out wheel, in order to better reflect the force of the meshing process between the teeth of the knock-out wheel and the suction hole of the seed-metering plate [21]. At the same time, we sought to ensure that the applied load torque does not suddenly change by using the STEP function to make the load act smoothly within 0.1 s, then set the corresponding function as STEP (time, 0, 0, 0.1, 20) and +STEP (time, 0.1, 0, 1, 0). The resulting variation curve of the load torque is presented in Figure 9. In addition, the working speed of the planter was set at 18 km/h, that is, the rotation speed of the seed-metering plate was 2.09 rad/s, the meshing movement time of the simulation model was set as 3 s, and the step size was set as 2000.

**Figure 8.** Parametric model of knock-out wheel and seed-metering plate.

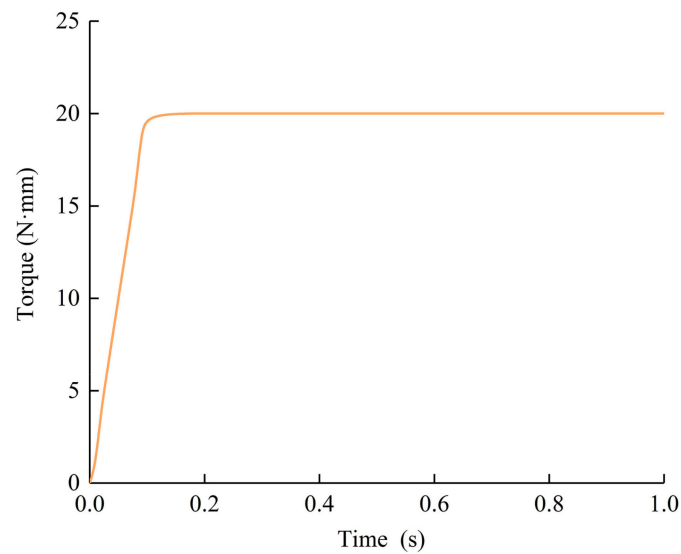


Figure 9. Variation curve of load torque.

2.6. Experimental Materials and Equipment

Experimental analyses of seeding performance were conducted at South China Agricultural University in Tianhe District, Guangzhou, China, using pelletized vegetable seeds produced by Weifang Agricultural Technology Co., Ltd. (Weifang, China) as the experimental material. Its thousand-grain mass was 23.5 g, with a sphericity of 97.6%, and an average particle size range of 4.0–4.2 mm. The seeding experiment device mainly comprised an air-suction seed-metering device, an AC drive motor, a vortex air pump, a frequency converter, a governor, a seed guide tube, an intelligent pressure anemometer, and a photoelectric sensor. The simplicity of the device does not affect its working function, as shown in Figure 10.

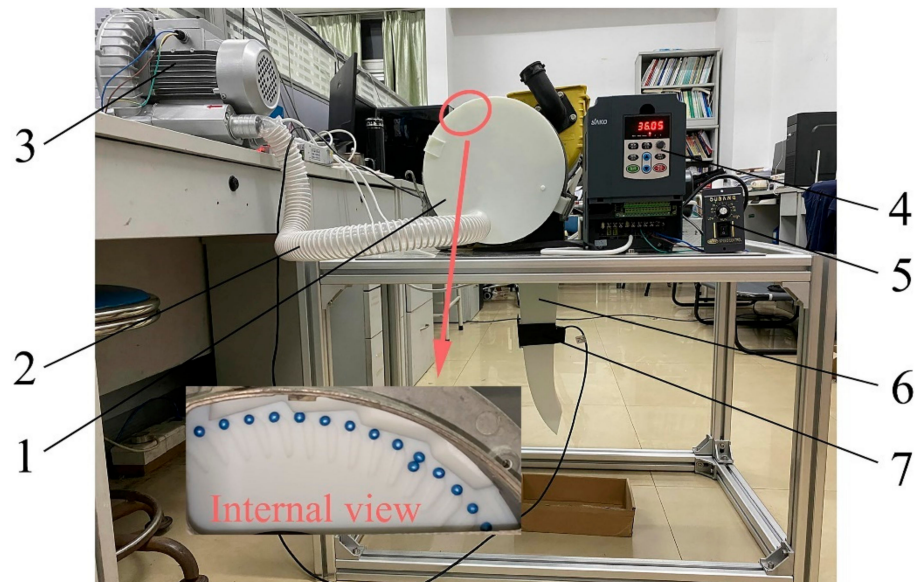


Figure 10. Seeding performance experimental device: (1) Air-suction seed-metering device; (2) pneumatic tube; (3) vortex air pump; (4) frequency converter; (5) governor; (6) seed guide tube; (7) laser sensor.

2.7. Experimental Performance Evaluation Indicators

Results from the theoretical analysis of the working process of the air-suction seed-metering device showed that the seed-throwing angle, working speed, and negative pres-

sure significantly influence its seeding performance. Therefore, the seed-throwing angle, working speed, and negative pressure were selected as the factors influencing seeding performance. At the same time, based on the above-mentioned theoretical design parameters and simulation model, we aimed to optimize the seed-metering plate and seed-unloading mechanism of the air-suction seed-metering device using 3D printing technology. Thereafter, we selected the qualified index (Y_1), multiple index (Y_2), and missing index (Y_3) as performance indexes for evaluating the working quality and stability of the seed-metering device, according to the agronomic requirements of vegetable seeding working and the National Standard of P.R.C. [22]. This was calculated using the equations below:

$$\begin{cases} Y_1 = \frac{z_1}{Z} \times 100\% \\ Y_2 = \frac{z_2}{Z} \times 100\% \\ Y_3 = \frac{z_3}{Z} \times 100\% \end{cases} \quad (11)$$

where z_1 is the number of seeds with inter-seed spacing bigger than half the theoretical value and smaller than 1.5 times the theoretical value; z_2 is the number of seeds with inter-seed spacing smaller than half the theoretical value; z_3 is the number of seeds with inter-seed spacing smaller than 1.5 times the theoretical value; while Z is the total number of seeds statistically involved. The laser sensor external to the seed guide tube was used to record time information of the seed falling for the calculation of evaluation indicators of seed-metering performance [23,24]. The laser sensor detection model is shown in Figure 11.

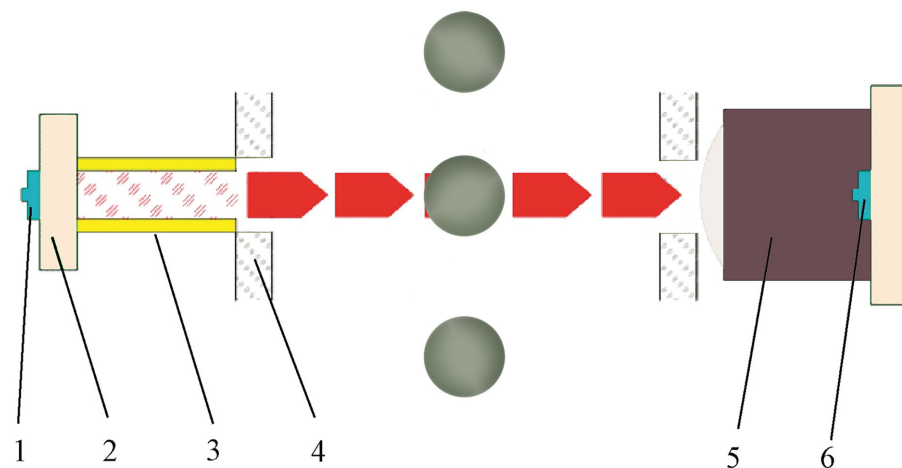


Figure 11. Laser sensor monitoring model: (1) modulation tube; (2) circuit board; (3) laser emission tube; (4) transparent plate; (5) lens; (6) receiving tube.

2.8. One-Factor Experimental Design

In order to improve the seeding performance of the seed-metering device, we analyzed the influence law of various experimental factors on seeding performance and obtained a reasonable range of orthogonal experimental factors. Consequently, we selected the seed-throwing angle, working speed, and negative pressure as experimental factors for the seeding performance experiment. The theoretical plant spacing was set at 0.15 m, resulting in the collection of 240 seeds for statistics in each group, with each group repeated three times. The value of each factor and the codes of the corresponding level in one-factor experiments are shown in Table 2.

Table 2. Experimental factors and level codes of one-factor experiments.

Level Code	Experimental Factors		
	Seed-Throwing Angle (°)	Working Speed (km/h)	Negative Pressure (kPa)
1	0	6	1.5
2	10	10	2.5
3	20	14	3.5
4	30	18	4.5
5	40	22	5.5

2.9. Multi-Factor Experimental Design

To determine the optimal combination of seeding performance parameters, a quadratic orthogonal rotation combination experiment was carried out on the basis of a one-factor experiment. Orthogonal experimental design can achieve results equivalent to a large number of comprehensive experiments with the least number of experiments. Therefore, the application of orthogonal table design experiments is an efficient, fast, and economical multi-factor experimental design method [25–27]. Specifically, the seed-throwing angle (x_1), working speed (x_2), and negative pressure (x_3) were selected as experimental factors, while the qualified index (Y_1), multiple index (Y_2), and missing index (Y_3) were selected as experimental performance evaluation indicators. A summary of values for each factor and the codes of the corresponding level in multi-factor experiments are presented in Table 3.

Table 3. Experimental factors and level codes of multi-factor experiments.

Level Code	Experimental Factors		
	Seed-Throwing Angle (°)	Working Speed (km/h)	Negative Pressure (kPa)
−1.682	0	10	1.5
−1	6	11.6	2.1
0	15	14	3
1	24	16.4	3.9
1.682	30	18	4.5

3. Results and Discussion

3.1. Numerical Simulation Analysis of Suction Hole Airflow Field Based on DEM-CFD Coupling

The Fluent post-processing tool was employed to generate fluid domain velocity vector diagrams of the suction holes A, B, and C, as shown in Figure 12. The vortex phenomenon in the fluid domain causes a certain degree of pressure loss and increases energy consumption, consequently impacting both the flow field stability and the adsorption effect of seeds. The following observations are presented in Figure 12: The A-type suction hole structure shows a significant vortex generation in the fluid domain; the vortex phenomenon was improved in different degrees of the B-type suction hole structure and C-type suction hole structure.

Turbulent kinetic energy is the carrier that reflects the magnitude of turbulent pulsation energy [28]. Assessment of the turbulent kinetic energy of the suction hole axis line allowed for further analysis of the variation of turbulent kinetic energy inside the suction holes with different structures. The turbulent kinetic energy variation of the suction hole axis line is shown in Figure 13. The overall turbulent kinetic energy on the axis line of the B-type suction hole was larger compared to that of the A-type and C-type suction holes (Figure 13). This means that the kinetic energy of the sub-particles around the inlet flow field of the B-type suction hole is larger. Since the kinetic energy between the sub-particles is transferred through the cohesive bond, it can be deduced that the adsorption effect of the seeds in the B-type suction hole was the best under the same boundary conditions.

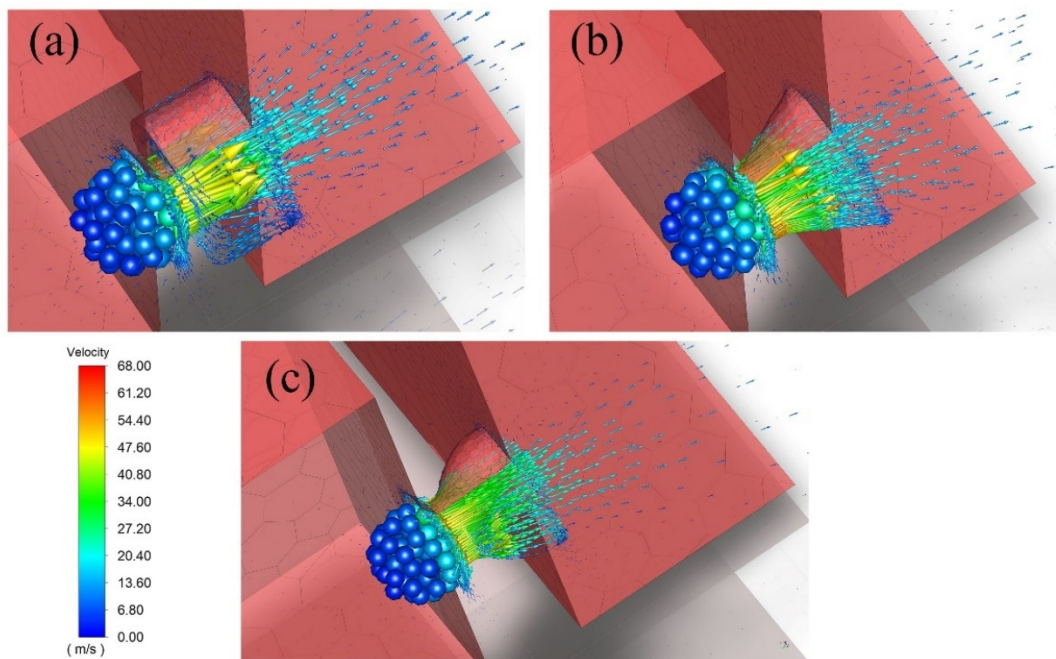


Figure 12. Velocity vector diagram of the suction hole fluid domain. (a) A; (b) B; (c) C.

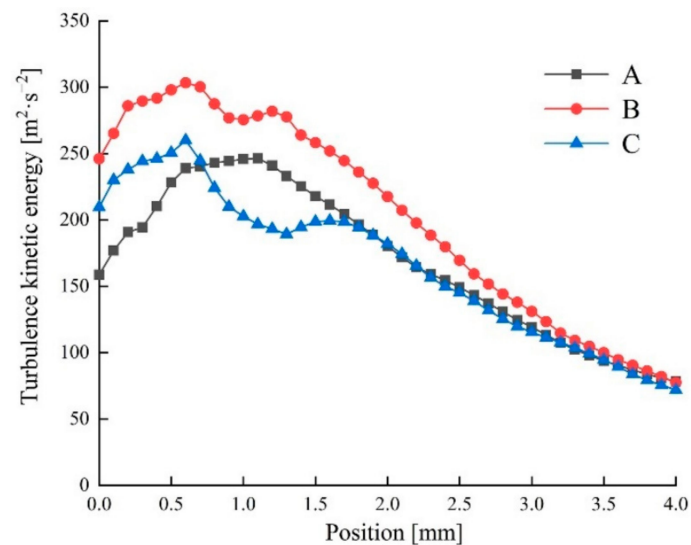


Figure 13. Turbulent kinetic energy variation of the suction hole axis line.

Assessment of pressure and velocity of the suction hole axis line allowed for further analysis of the variation of pressure and velocity inside the suction holes with different structures. A scatter diagram of the pressure and velocity is shown in Figure 14.

The main basis for quality evaluation of the suction hole structure is the coupling force of the suction hole on the seed. The EDEM post-processing tool was employed to derive the coupling force on the seed particles along the axis of the suction hole, as shown in Figure 14. Figure 14 shows that when the seed particles are stably adsorbed to the suction holes (after 0.2 s of coupling simulation), the coupling force of the C-type suction hole to the seed particles is the smallest, with an average of 0.015 N, while the coupling force of the B-type suction hole to the seed particles is the largest, with an average of 0.029 N. The B-type suction hole structure demonstrates relatively upstanding seed suction performance in the turbulent kinetic energy and particle coupling force. Therefore, in designing the suction hole structure of the seed-metering plate, the suction hole structure

in the form of the B-type is preferred to ensure more effective and stable seed adsorption by the seed-metering device.

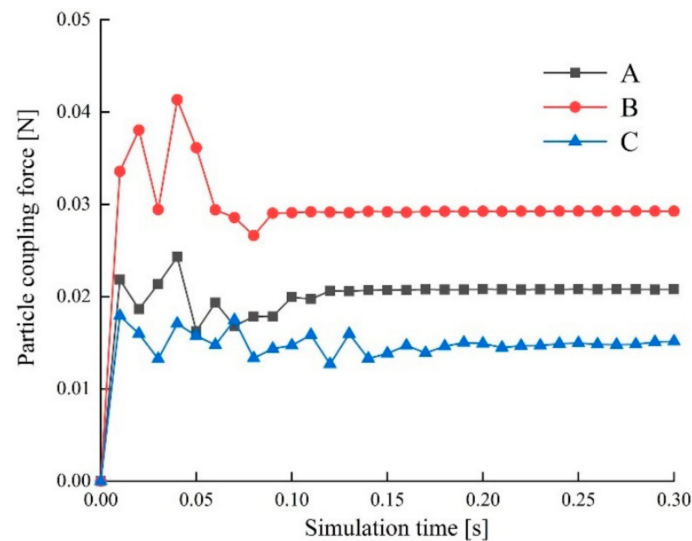


Figure 14. The coupling force variation on the seed particles along the axis of the suction hole.

By smoothly ejecting the impurities or seeds on the front surface of the seed-metering plate, one becomes certain that the knock-out wheel tooth is inserted into the suction hole on the rear surface of the seed-metering plate. The spherical design is adopted to increase the tooth top height to 4 mm. The design of the tooth profile of the knock-out wheel matched the B-type suction hole (Figure 15). The knock-out wheel was rotated clockwise by half of the included angle between adjacent teeth (22.5°). As demonstrated in Figure 15a,b, the knock-out wheel teeth do not interfere with the suction hole at the beginning and end of the meshing position. This is a preliminary verification of the rationality of the designed knock-out wheel tooth profile.

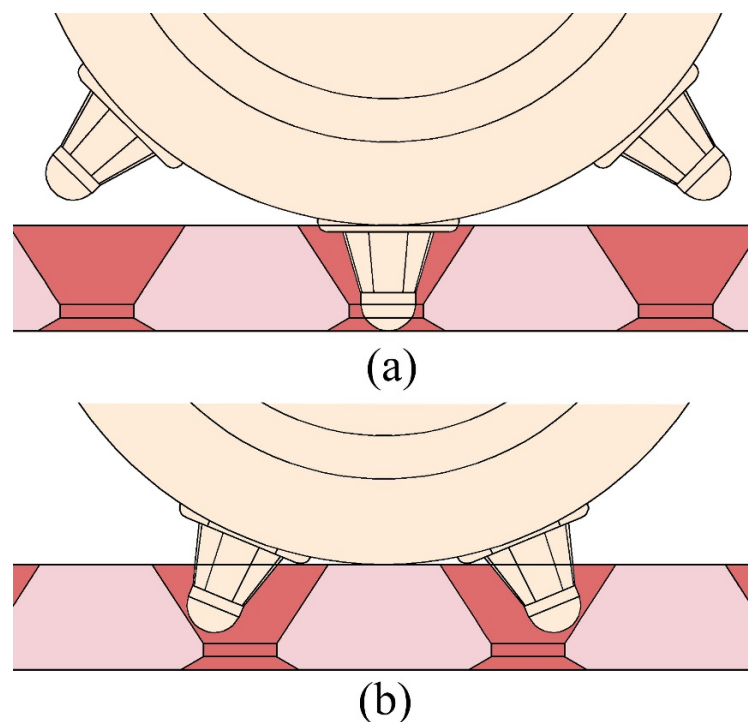


Figure 15. Knock-out wheel tooth profile design. (a) initial; (b) rotation 22.5° .

3.2. Analysis of the Meshing Performance between Knock-Out Wheel and Seed-Metering Plate

Motion simulation experiments of the parametric model of the knock-out wheel and seed-metering plate were conducted to obtain the meshing condition between the knock-out wheel and the seed-metering plate before upgrading the physical prototype. This reduced the costs of R&D and updates. The animation demonstration function of the Adams Post-Processor was applied to assess the movement of the knock-out wheel teeth and the suction hole during the meshing process and to check for any interference throughout the whole meshing process. Results revealed that the knock-out wheel teeth and the suction holes operated stably during the meshing process, with no interference between the two structures. There was no interruption due to calculation errors in the simulation process, which verified the rationality of the designed knock-out wheel tooth profile.

The Adams Post-Processor was employed to determine the force between the knock-out wheel teeth and the suction hole within 0~1 s and explore the meshing performance between them. Figure 16 shows the force variation curve during the meshing process. It is notable that the meshing force curve escalated rapidly in a short time and then fluctuated periodically (Figure 16a). In the initial stage, the gear teeth of the knock-out wheel were tangent to the suction hole of the seed-metering plate, with no contact between the gear teeth and the internal structure of the suction hole. Subsequently, the angular velocity of the seed-metering plate increased from 0 rad/s to 2.09 rad/s instantaneously, which caused a larger impact force, instantaneously increasing the meshing force to a larger value. In addition, before the 0.1 s stage, an increase in load torque continuously increased the meshing force between the gear teeth and the suction hole with notable fluctuations. After the 0.1 s stage, the load torque attained a predetermined value, and the meshing force between the gear teeth and the suction hole seized increased. As such, the fluctuation trend began to show a stable periodic state. The fluctuation period of the meshing force was calculated as 0.05 s using the ADMAS Post-Processor module, which concurred with the theoretical meshing period calculated in Section 2.3.2. The radial force gradually increased with the increase in the load torque and fluctuated periodically after 0.1 s (Figure 16b), similar to the overall variation of the meshing force. Of note, the variation of the radial force reflects the periodic force of the gear teeth relative to the suction hole in the vertical direction. Therefore, increasing the meshing stability between the gear teeth and the suction hole required the installation of a spring in the vertical direction and the use of spring force to improve the negative impact due to the periodically fluctuating radial force. As demonstrated in Figure 16c, the periodic change trend of the axial force was similar to the radial force, but the value was relatively small, providing evidence that the knock-out wheel was also subject to certain periodic impacts on the axial direction during the meshing process. The knock-out wheel was designed to be slidable in the axial direction to alleviate the impact force along the axial direction of the knock-out wheel during the meshing process. This subsequently improved the negative impact of the axial periodic impact on the knock-out wheel. In this view, a seed-unloading mechanism was designed (Figure 17).

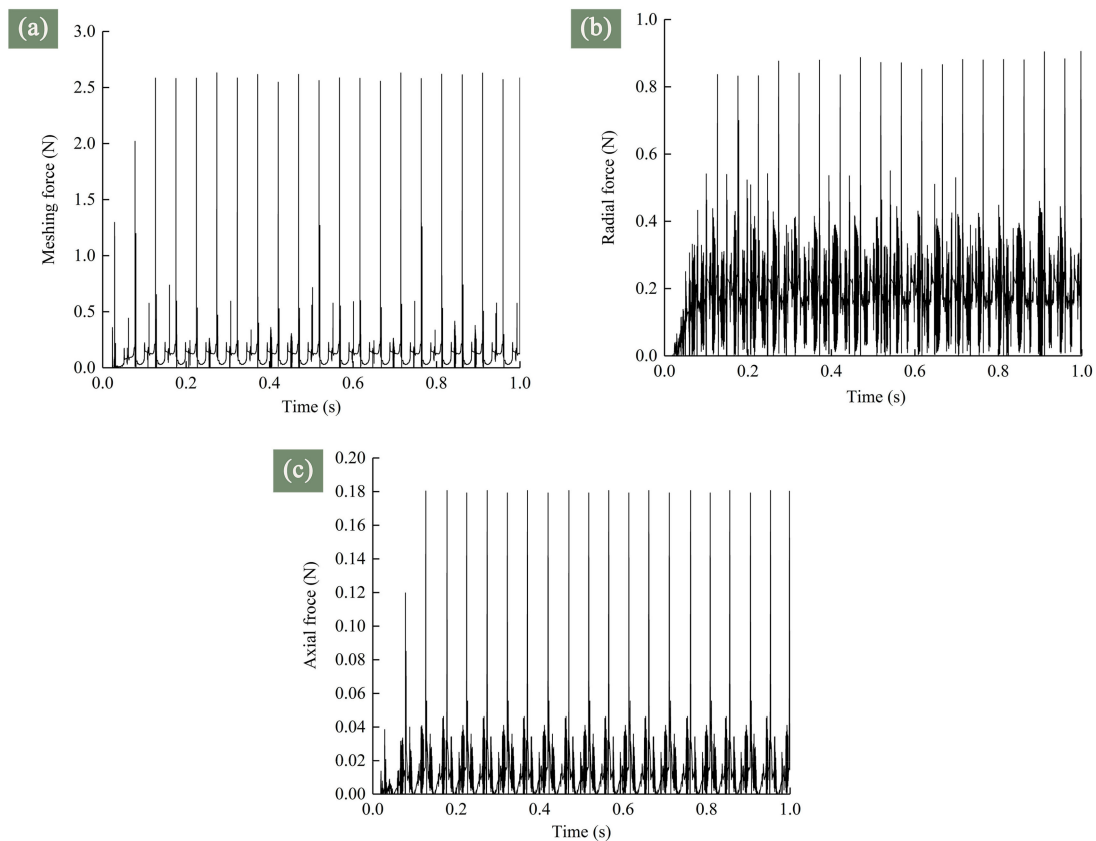


Figure 16. The force variation curve during the meshing process: (a) Meshing force, (b) radial force, (c) axial force.

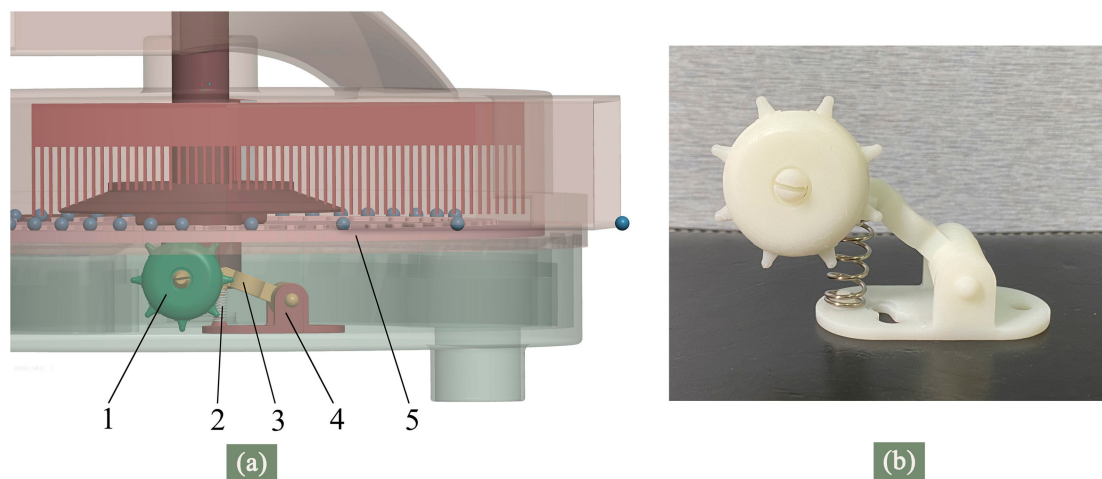


Figure 17. Seed unloading mechanism. (a) Schematic diagram, (b) 3D printing physical object. (1) seed-ejecting wheel; (2) spring; (3) support rod; (4) base; (5) seed-metering plate.

3.3. One-Factor Experimental Results

3.3.1. The Influence of Working Speed on Seeding Performance

To analyze the influence of working speed on various experimental indicators, a seeding angle of 20° and negative pressure of 3.5 kPa were selected. Five levels of the working speed, 6 km/h, 10 km/h, 14 km/h, 18 km/h, and 22 km/h, were selected, and three experiments were performed on each level. The variation law of the seeding performance

evaluation index with the working speed was obtained by analyzing the experimental results (Figure 18).

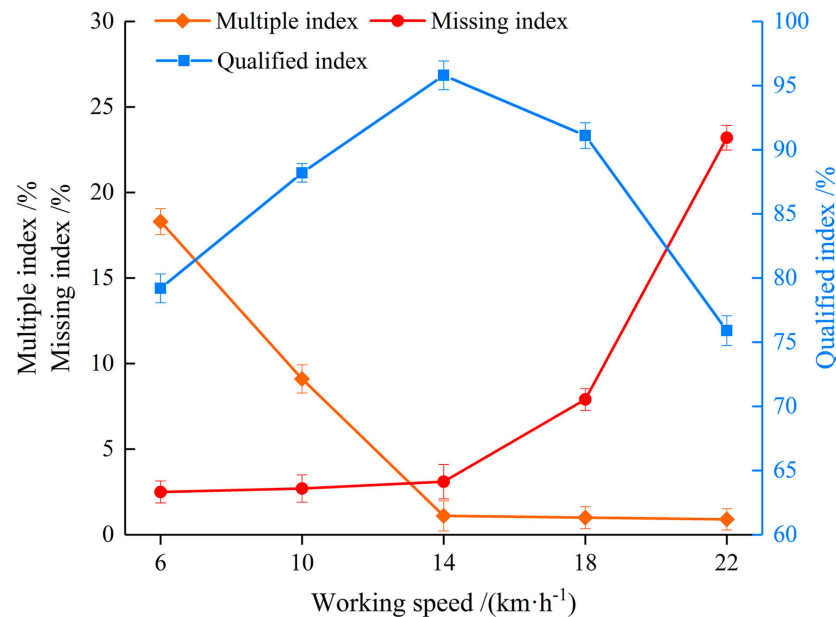


Figure 18. The influence of working speed on seeding performance evaluation index.

As demonstrated in Figure 18, the qualified index shows a trend of first increasing and then decreasing with an increase in working speed. On the other hand, the multiple index shows a gradually decreasing trend, and the missing index shows a gradually increasing trend. At a 6 km/h working speed, the multiple index is the highest and the missing index is the lowest. To explain this, a low rotation speed of the seed-metering plate results in a prolonged stay of the suction hole in the seed-filling area. As such, there is sufficient time for seeds to be adsorbed by the suction hole. With the increase in the rotation speed of the seed-metering plate, the qualified index gradually increased, the multiple index also decreased sharply, and the missing index showed a slow upward trend as a whole. These observations are because an increase in the rotation speed of the seed-metering plate improved the dispersion of seed groups. As a result, the probability of the suction holes to absorb seeds increased, reducing the negative impact of the higher multiple index caused by the increase in the rotation speed of the seed-metering plate. When the working speed is too high, the residence time of the suction holes in the seed-filling area becomes too short. In this regard, some seeds cannot be adsorbed in a timely manner by the suction holes, which then increases the missed seeding phenomenon and decreases the qualified index.

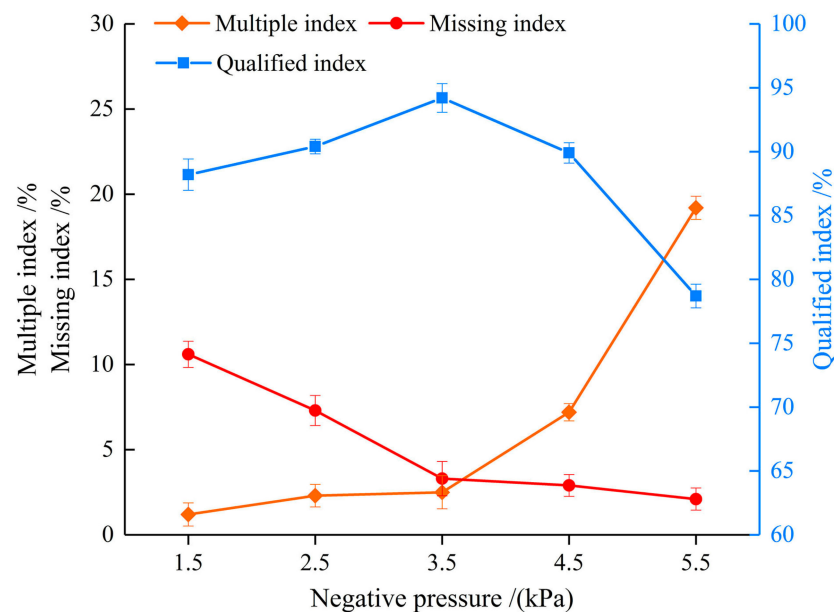
The results of the above-mentioned one-factor experiments were processed in IBM SPSS(r) Statistics V 25.0 (Armonk, NY, USA). Table 4 shows the results of variance analysis (ANOVA) of the influence of the working speed on the seeding performance. It is notable that the working speed extremely significantly influences each seeding performance indicator. According to the Chinese National Standard JB/T 10293-2013 ‘Specifications for Single Seed drills (Precision Drills)’ [29], a qualified index of no less than 80%, a multiple index of no more than 15%, and a missing index of no more than 8% are acceptable. The reasonable value range of the working speed can be obtained as 10–18 km/h.

Table 4. Results of ANOVA of the working speed on seeding performance indicators.

Source of Variation		Qualified Index		Multiple Index		Missing Index		
		SS	Sig.	SS	Sig.	SS	Sig.	
Between groups	(Combined)	825.560	0.000	710.640	0.000	1056.791	0.000	
	Linear term	Contrast	3.888	0.045	555.474	0.000	719.320	0.000
		Deviation	821.672	0.000	155.166	0.000	337.470	0.000
	Quadratic term	Contrast	788.667	0.000	145.936	0.000	269.040	0.000
Deviation		33.005	0.000	9.230	0.006	68.430	0.000	
Within groups		8.153		5.079		5.753		
Total		833.713		715.719		1062.544		

3.3.2. The Influence of Negative Pressure on Seeding Performance

To analyze the influence of negative pressure on various experimental indicators, a seed-throwing angle of 20° and a working speed of 14 km/h were selected. In this regard, five levels of negative pressure, 1.5 kPa, 2.5 kPa, 3.5 kPa, 4.5 kPa, and 5.5 kPa, were selected, and three experiments were performed on each level. The variation law of the seeding performance evaluation index with the negative pressure was obtained by analyzing the experimental results (Figure 19).

**Figure 19.** The influence of negative pressure on seeding performance evaluation index.

As demonstrated in Figure 19, the qualified index shows a trend of first increasing and then decreasing with increasing negative pressure. At a low negative pressure level, the multiple index remains low and the multiple index begins to rise sharply following an increase in the negative pressure to 3.5 kPa. At a 1.5 kPa negative pressure, the missing index reached the highest value and then began to decline sharply. This is mainly because the state of the seeds being adsorbed by the suction holes is unstable when the negative pressure is low. At this time, a higher phenomenon of missed seeding is realized. However, the phenomenon of missed seeding decreases, and the qualification index increases with the increase in negative pressure. When the negative pressure is too large, the ability of the suction hole to adsorb seeds is too strong, therefore multiple seeds can easily be adsorbed, which increases the reseeding phenomenon and decreases the qualified index. SPSS software was employed to process the results of the above-mentioned one-factor experiments. Results of ANOVA of the influence of negative pressure on the seeding performance evaluation indicators are shown in Table 5. It is notable that the negative pressure extremely significantly influences each seeding performance indicator, and the reasonable value range of the negative pressure is 1.5–4.5 kPa.

Table 5. Results of ANOVA of the negative pressure on seeding performance indicators.

Source of Variation			Qualified Index		Multiple Index		Missing Index	
			SS	Sig.	SS	SS	Sig.	SS
Between groups	(Combined)		401.737	0.000	674.827	0.000	157.051	0.000
	Linear term	Contrast	114.075	0.000	505.120	0.000	138.245	0.000
		Deviation	287.662	0.000	169.706	0.000	18.805	0.002
	Quadratic term	Contrast	260.006	0.000	148.972	0.000	15.604	0.000
		Deviation	27.656	0.001	20.735	0.000	3.202	0.012
Within groups			8.420		4.567		5.833	
Total			410.157		679.393		162.884	

3.3.3. The Influence of Seed-Throwing Angle on Seeding Performance

To analyze the influence of the seed-throwing angle on various experimental indicators, a working speed of 14 km/h and the negative pressure of 3.5 kPa were selected. In this regard, five levels of the seed-throwing angle, 0°, 10°, 20°, 18°, and 22°, were selected, and three experiments were performed on each level. The variation law of the seeding performance evaluation index with the seed-throwing angle was obtained by analyzing the experimental results (Figure 20).

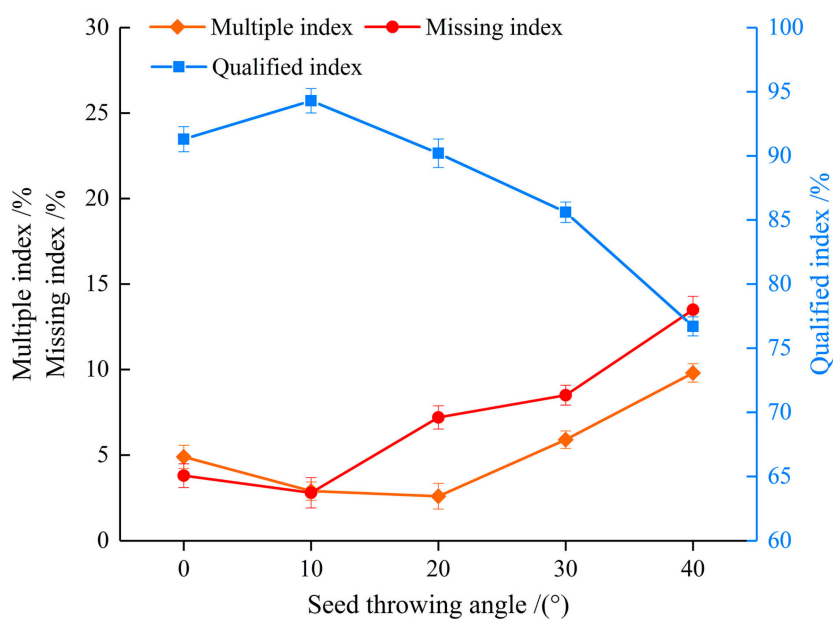


Figure 20. The influence of seed-throwing angle on seeding performance evaluation index.

As demonstrated in Figure 20, a seed-throwing angle within the range of 0–20° resulted in a qualified index of no less than 90%, a missing index of no higher than 7.2%, and a multiple index of no higher than 2.6%. With the increase in the seed-throwing angle, the qualified index first increases rapidly and then decreases sharply after reaching the highest point. At a 10° seed-throwing angle, the qualified index rises to the highest point at 94.3%. However, the qualified index drops to the lowest, at 76.7%, when the seed-throwing angle is 40°. SPSS software was employed to process the results of the above-mentioned one-factor experiments. Results of ANOVA of the influence of seed-throwing angle on the seeding performance evaluation indicators are shown in Table 6. It is notable that the seed-throwing angle extremely significantly influences each seeding performance indicator, and a reasonable value range of the seed-throwing angle is 0–30°.

Table 6. Results of ANOVA of the seed-throwing angle on seeding performance indicators.

Source of Variation			Qualified Index		Multiple Index		Missing Index	
			SS	Sig.	SS	SS	Sig.	SS
Between groups	(Combined)		561.531	0.000	102.887	0.000	219.423	0.000
	Linear term	Contrast	427.896	0.000	49.408	0.000	191.016	0.000
		Deviation	133.634	0.000	53.478	0.000	28.406	0.000
	Quadratic term	Contrast	126.534	0.000	51.926	0.000	17.486	0.000
Deviation		7.101	0.041	1.552	0.045	10.920	0.003	
Within groups			7.973		3.287		4.873	
Total			569.504		106.173		224.296	

3.4. Multi-Factor Experimental Results

The experimental plan and results of multi-factor experiments are shown in Table 7.

Table 7. The experimental plan and results of multi-factor experiments.

Experiment Number	Experimental Factors			Objective Functions		
	Seed-Throwing Angle x_1 (°)	Working Speed x_2 (km/h)	Negative Pressure x_3 (kPa)	Qualified Index Y_1 (%)	Multiple Index Y_2 (%)	Missing Index Y_3 (%)
1	15	10	3	88.4	9.3	2.3
2	0	14	3	91.3	5.2	3.5
3	6	16.4	2.1	93.8	3.7	2.5
4	15	18	3	92.3	0.8	6.9
5	6	11.6	3.9	92.5	2.3	5.2
6	15	14	1.5	91.7	4.2	4.1
7	6	16.4	3.9	94.9	0.9	4.2
8	15	14	4.5	92.2	5.4	2.4
9	15	14	3	95.2	2.7	2.1
10	15	14	3	95.8	2.3	1.9
11	15	14	3	96.5	0.1	3.4
12	15	14	3	96.3	1.6	2.1
13	24	16.4	3.9	90.1	7.8	2.1
14	24	11.6	3.9	89.2	9.4	1.4
15	15	14	3	96.5	0.2	3.3
16	6	11.6	2.1	89.4	10.5	0.1
17	24	11.6	2.1	89.7	8.5	1.8
18	30	14	3	91.2	6.9	1.9
19	15	14	3	96.1	1.8	2.1
20	24	16.4	2.1	91.5	3.1	5.4

3.4.1. ANOVA Results of the Qualified Index

Results of the multi-factor experiments were processed in Design Expert 11.0 software. Table 8 shows the results of ANOVA for the qualified index (Y_1); x_1 , x_2 , x_1^2 , x_2^2 , and x_3^2 extremely significantly influence the qualified index, whereas x_1x_3 significantly influence the qualified index. According to the results of ANOVA, the coding regression equation of the influence of the seed-throwing angle (x_1), working speed (x_2), and negative pressure (x_3) on the qualified index (Y_1) were obtained as follows:

$$Y_1 = 96.05 - 0.75x_1 + 1.18x_2 + 0.23x_3 - 0.51x_1x_2 - 0.76x_1x_3 - 0.36x_2x_3 - 1.6x_1^2 - 1.92x_2^2 - 1.35x_3^2 \quad (12)$$

Based on the results of the lack-of-fit test of the above regression equation, the p -value of the lack-of-fit term is greater than 0.5, which is not significant. These results demonstrate that the regression equation fits well with the experimental value of the qualified index, and a significant quadratic correlation exists between the qualified index and the above experimental factors.

Table 8. Results of ANOVA of the regression equation for the qualified index.

Source	Sum of Squares	Df	Mean Square	F-Value	p-Value
Model	132.48	9	14.72	20.15	<0.0001
x_1	7.72	1	7.72	10.57	0.0087
x_2	18.88	1	18.88	25.86	0.0005
x_3	0.7223	1	0.7223	0.9890	0.3434
x_1x_2	2.10	1	2.10	2.88	0.1207
x_1x_3	4.65	1	4.65	6.37	0.0302
x_2x_3	1.05	1	1.05	1.44	0.2579
x_1^2	36.78	1	36.78	50.36	<0.0001
x_2^2	52.89	1	52.89	72.41	<0.0001
x_3^2	26.27	1	26.27	35.96	0.0001
Residual	7.30	10	0.7304		
Lack of fit	6.05	5	1.21	4.83	0.0545
Pure error	1.25	5	0.2507		
Cor total	139.78	19			

3.4.2. ANOVA Results of the Multiple Index

Results of the multi-factor experiments were processed in Design Expert 11.0 software. Table 9 shows the results of ANOVA for the multiple index (Y_2); x_1 , x_2 , x_1x_3 , x_1^2 , x_2^2 , and x_3^2 extremely significantly influence the multiple index, whereas x_2x_3 significantly influence the multiple index. According to the results of ANOVA, the coding regression equation of the influence of the seed-throwing angle (x_1), working speed (x_2), and negative pressure (x_3) on the multiple index (Y_2) were obtained as follows:

$$Y_2 = 1.44 + 1.04x_1 - 2.16x_2 - 0.25x_3 + 0.15x_1x_2 + 2.08x_1x_3 + 1.15x_2x_3 + 1.68x_1^2 + 1.32x_2^2 + 1.24x_3^2 \tag{13}$$

Table 9. Results of ANOVA of the regression equation for the multiple index.

Source	Sum of Squares	Df	Mean Square	F-Value	p-Value
Model	198.31	9	22.03	15.79	<0.0001
x_1	14.89	1	14.89	10.67	0.0085
x_2	63.70	1	63.70	45.65	<0.0001
x_3	0.8372	1	0.8372	0.5999	0.4565
x_1x_2	0.1800	1	0.1800	0.1290	0.7270
x_1x_3	34.44	1	34.44	24.68	0.0006
x_2x_3	10.58	1	10.58	7.58	0.0204
x_1^2	40.55	1	40.55	29.06	0.0003
x_2^2	25.26	1	25.26	18.10	0.0017
x_3^2	22.00	1	22.00	15.76	0.0026
Residual	13.96	10	1.40		
Lack of fit	8.14	5	1.63	1.40	0.3605
Pure error	5.82	5	1.16		
Cor total	212.27	19			

Based on the results of the lack-of-fit test of the above regression equation, the p -value of the lack-of-fit term is greater than 0.5 ($p = 0.3605$), which is not significant. These results demonstrate that the regression equation fits well with the experimental value of the multiple index, and a significant quadratic correlation exists between the multiple index and the above experimental factors.

3.4.3. ANOVA Results of the Missing Index

Design Expert 11.0 software was employed to process the results of the multi-factor experiments. Table 10 shows the results of ANOVA for the missing index (Y_1); x_2 and x_1x_3 extremely significantly influence the missing index, whereas x_1x_2 , x_2x_3 , and x_2^2 significantly influence the missing index. According to the results of ANOVA, the coding regression

equation of the influence of the seed-throwing angle (x_1), working speed (x_2), and negative pressure (x_3) on the missing index (Y_3) were obtained as follows:

$$Y_3 = 2.51 - 0.29x_1 + 0.98x_2 + 0.02x_3 + 0.36x_1x_2 - 1.31x_1x_3 - 0.79x_2x_3 - 0.08x_1^2 + 0.59x_2^2 + 0.11x_3^2 \quad (14)$$

Table 10. Results of ANOVA of the regression equation for the missing index.

Source	Sum of Squares	Df	Mean Square	F-Value	p-Value
Model	39.58	9	4.40	5.20	0.0084
x_1	1.17	1	1.17	1.38	0.2677
x_2	13.22	1	13.22	15.62	0.0027
x_3	0.0042	1	0.0042	0.0050	0.9450
x_1x_2	1.05	1	1.05	1.24	0.2912
x_1x_3	13.78	1	13.78	16.28	0.0024
x_2x_3	4.96	1	4.96	5.86	0.0360
x_1^2	0.0919	1	0.0919	0.1086	0.7486
x_2^2	5.05	1	5.05	5.96	0.0347
x_3^2	0.1892	1	0.1892	0.2235	0.6465
Residual	8.46	10	0.8465		
Lack of fit	6.18	5	1.24	2.70	0.1499
Pure error	2.29	5	0.4577		
Cor total	48.05	19			

Based on the results of the lack-of-fit test of the above regression equation, the p -value of the lack-of-fit term is greater than 0.5 ($p = 0.1499$), which is not significant. These results demonstrate that the regression equation fits well with the experimental value of the missing index, and a significant quadratic correlation exists between the missing index and the above experimental factors.

3.4.4. Results of Response Surface Methodology (RSM) of Experimental Indicators

In order to visually analyze the influence of experimental factors on experimental indicators, in Design Expert 11.0 software, the seed-throwing angle, working speed, and negative pressure were set to zero in the sequence. Next, the influence of the other two experimental factors on the experimental indicators was examined. The response surface and the corresponding projection contour of the influence of experimental factors on the qualified index are shown in Figure 21.

According to the results of the influence of experimental factors on the qualified index (Y_1), the following observations were made: (i) At a seed-throwing angle of 15° and constant working speed, the qualified index increases first and then decreases with increasing negative pressure, and the optimal range of the negative pressure is 2.6–3.5 kPa. (ii) At a seed-throwing angle of 15° and constant negative pressure, the qualified index increases first and then decreases with an increase in working speed, and the optimal range of the working speed is 13.6–15.8 km/h. (iii) A working speed of 14 km/h and a constant seed-throwing angle causes the qualified index to first increase and then decrease with increasing negative pressure, and the optimal range of the negative pressure is 2.7–3.6 kPa. (iv) A working speed of 14 km/h and constant negative pressure causes the qualified index to first increase and then decrease with an increasing seed-throwing angle, and the optimal range of the seed-throwing angle is 9 – 16° . (v) At a negative pressure of 3 kPa and a constant seed-throwing angle, the qualified index increases first and then decreases with increasing working speed, and the optimal range of the working speed is 13.8–16.0 km/h. (vi) A negative pressure of 3 kPa and constant working speed causes the qualified index to increase first and then decrease with an increasing seed-throwing angle, and the optimal range of the seed-throwing angle is 7 – 18° .

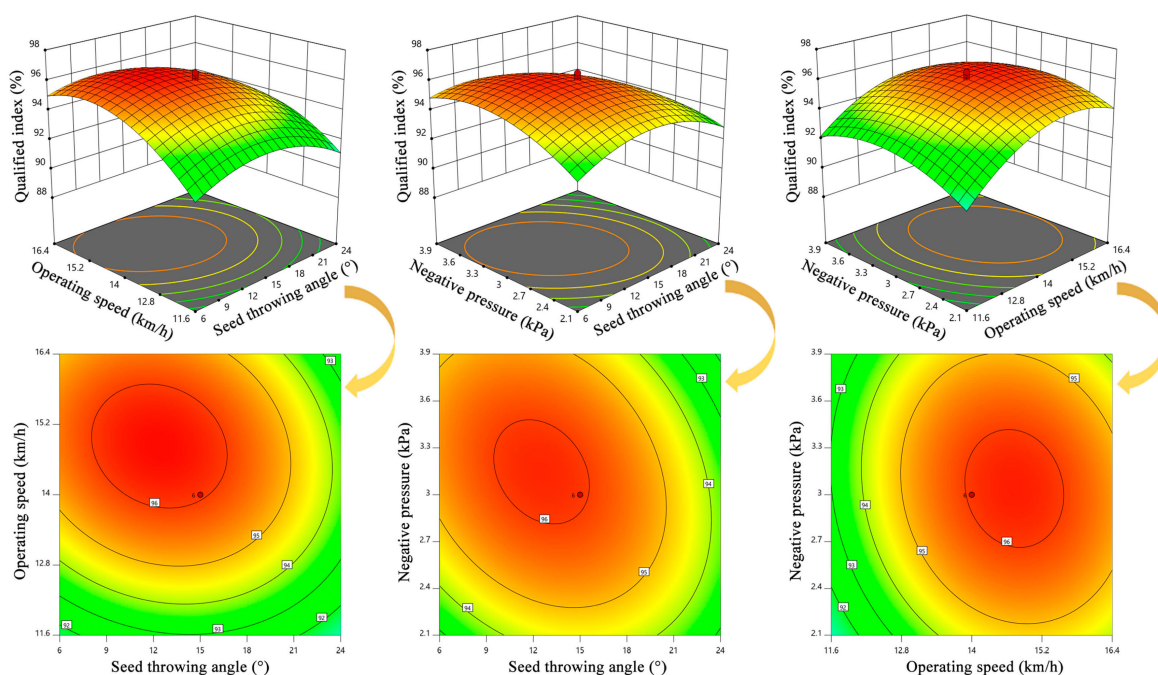


Figure 21. The RSM results of the influence of experimental factors on the qualified index.

The RSM results of the influence of experimental factors on the qualified index revealed that the working speed is the main influencing factor on the qualified index in the interaction of the working speed with the negative pressure. Moreover, the working speed is the main influencing factor on the qualified index in the interaction of the working speed with the seed-throwing angle. Lastly, the seed-throwing angle is the main influencing factor on the qualified index in the interaction of the seed-throwing angle with the negative pressure.

The response surface and the corresponding projection contour of the influence of experimental factors on the multiple index are shown in Figure 22. According to the results of the influence of experimental factors on the multiple index (Y_2), the following observations were made: (i) At a seed-throwing angle of 15° and a constant working speed, the multiple index decreases first and then increases with increasing negative pressure, and the optimal range of the negative pressure is 2.1–3.9 kPa. (ii) At a seed-throwing angle of 15° and constant negative pressure, the multiple index demonstrates a gradually decreasing trend with the increase in the working speed, and the optimal range of the working speed is 13.6–16.4 km/h. (iii) At a working speed of 14 km/h and a constant seed-throwing angle, the multiple index decreases first and then increases with increasing negative pressure, and the optimal range of the negative pressure is 2.4–3.9 kPa. (iv) At a working speed of 14 km/h and constant negative pressure, the multiple index decreases first and then increases with an increasing seed-throwing angle, and the optimal range of the seed-throwing angle is $6\text{--}19^\circ$. (v) At a negative pressure of 3 kPa and a constant seed-throwing angle, the multiple index shows a gradually decreasing trend with the increase in the working speed, and the optimal range of the working speed is 13.8–16.0 km/h. (vi) At a negative pressure of 3 kPa and a constant working speed, the multiple index shows an overall increasing trend with the increase in the seed-throwing angle, and the optimal range of the seed-throwing angle is $6\text{--}20^\circ$.

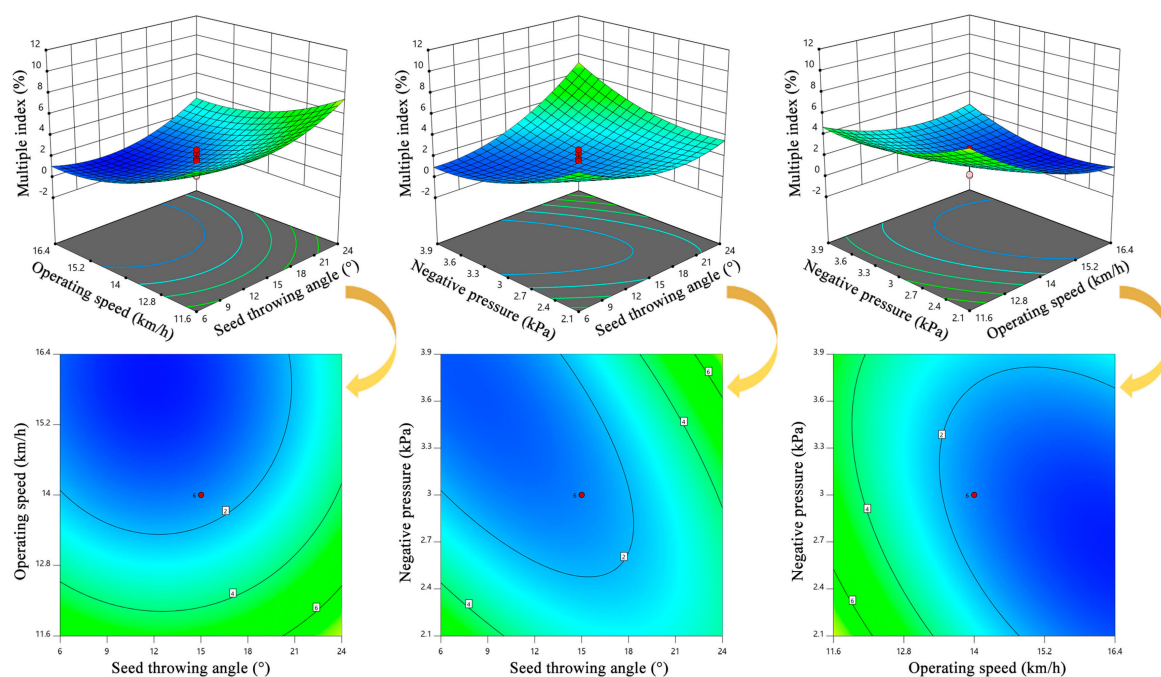


Figure 22. The RSM results of the influence of experimental factors on the multiple index.

The RSM results of the influence of experimental factors on the multiple index demonstrated the working speed to be the main influencing factor on the multiple index in the interaction between working speed and negative pressure. In addition, the working speed is the main influencing factor on the multiple index in the interaction between the working speed and the seed-throwing angle. Lastly, the seed-throwing angle is the main influencing factor on the multiple index in the interaction between the seed-throwing angle and negative pressure.

The response surface and the corresponding projection contour of the influence of experimental factors on the missing index are shown in Figure 23. According to the results of the influence of experimental factors on the missing index (Y_3), the following observations were made: (i) At a seed-throwing angle of 15° and a constant working speed, the missing index shows a slowly decreasing trend with the increase in the negative pressure, and the optimal range of the negative pressure is 2.1–3.9 kPa. (ii) At a seed-throwing angle of 15° and constant negative pressure, the missing index shows a gradually increasing trend with the increase in the working speed, and the optimal range of the working speed is 11.6–15.2 km/h. (iii) At a working speed of 14 km/h and a constant seed-throwing angle, the missing index shows a slowly decreasing trend with the increase in the negative pressure, and the optimal range of the negative pressure is 2.1–3.9 kPa. (iv) At a working speed is 14 km/h and constant negative pressure, the missing index shows a gradually decreasing trend with the increase in the seed-throwing angle, and the optimal range of the seed-throwing angle is 6 – 24° . (v) At a negative pressure of 3 kPa and a constant seed-throwing angle, the missing index shows a gradually increasing trend with the increase in the working speed, and the optimal range of the working speed is 11.6–14.2 km/h. (vi) At a negative pressure of 3 kPa and a constant working speed, the missing index shows a slowly increasing trend with the increase in the seed-throwing angle, and the optimal range of the seed-throwing angle is 11.6 – 13.8° .

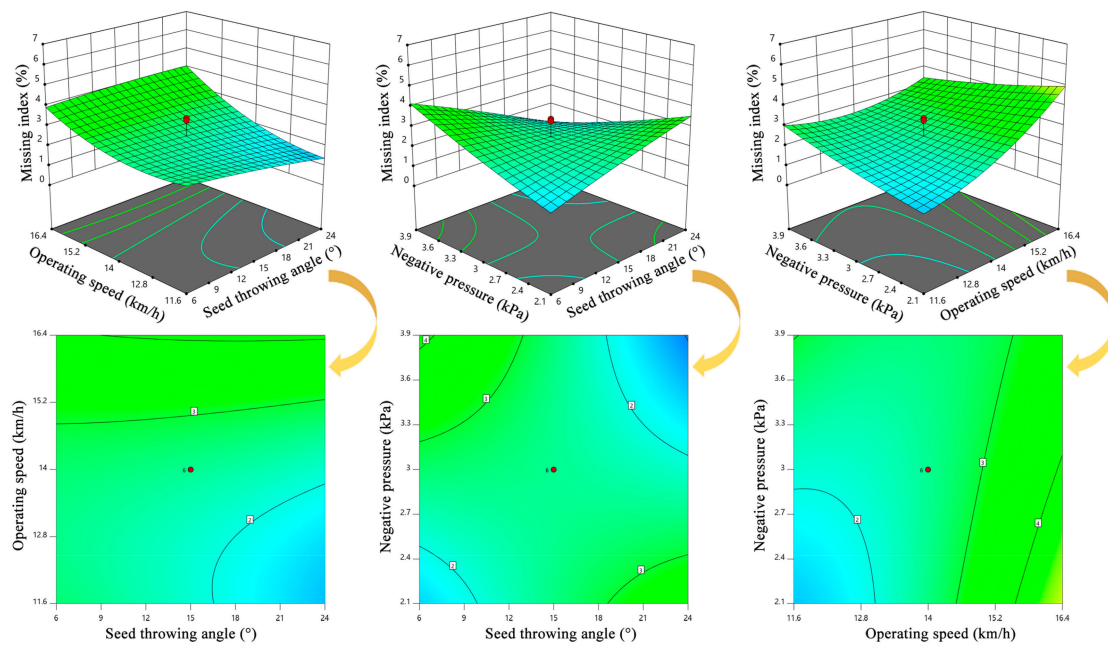


Figure 23. The RSM results of the influence of experimental factors on the missing index.

The RSM results of the influence of experimental factors on the missing index showed that the working speed is the main factor affecting the missing index in the interaction between the working speed and the negative pressure. In addition, the working speed is the main influencing factor on the missing index in the interaction between the working speed and the seed-throwing angle. Lastly, the seed-throwing angle is the main influencing factor on the missing index in the interaction between the seed-throwing angle and negative pressure.

3.4.5. The Optimal Parameter Combination of Experimental Factors

The experimental factors and the interaction between the experimental factors greatly influenced the seeding performance of the air-suction seed-metering device. Considering the highest-qualified index, the lowest missing index, and multiple index as the optimization objectives, the optimal parameter combination of experimental factors was determined. This was followed by a multi-objective optimization analysis of the experimental factors of the air-suction seed-metering device. The objective function and constraint conditions were established as follows:

$$\begin{cases} \max Y_1(x_1, x_2, x_3) \\ \min Y_2(x_1, x_2, x_3) \\ \min Y_3(x_1, x_2, x_3) \\ s.t. \begin{cases} 0^\circ \leq x_1 \leq 30^\circ \\ 10 \text{ km/h} \leq x_2 \leq 18 \text{ km/h} \\ 1.5 \text{ kPa} \leq x_3 \leq 30 \text{ kPa} \end{cases} \end{cases} \quad (15)$$

The above equations were solved employing the optimization module in Design Expert 11.0 software. After rounding, the optimal combination of experimental factors was revealed as follows: The seed-throwing angle: 13° ; the working speed: 14.5 km/h; the negative pressure: 3.1 kPa. The corresponding experimental indicators are as follows: The qualified index: 96.3%; the multiple index: 0.9%; the missing index: 2.8%. The seeding performance verification experiments of the seed-metering device were performed based on the optimized parameter values. Results of the verified experiments are shown in Table 11. The experimental results were consistent with the above optimization results as

follows: Average value of qualified index: 95.9%; the average value of multiple index: 1.2%; the missing index: 2.9%.

Table 11. Results of the verified experiments.

Number	Qualified Index	Multiple Index	Missing Index
1	95.1%	1.4%	3.5%
2	96.6%	1.1%	2.3%
3	95.3%	1.3%	3.4%
4	96.7%	0.9%	2.4%
5	95.8%	1.3%	2.9%
Average value	95.9%	1.2%	2.9%

4. Conclusions

The key structural parameters of the seed metering plate were analyzed and determined, then we established an adsorption mechanics model of the seed during the migration process and designed the key structure of the air-suction seed-metering device with the aim of improving the uniformity of high-speed direct seeding of vegetables.

Through the DEM-CFD coupling method, we analyzed the influence of the law of seeds on the change of the flow field with different hole types. Results showed that the turbulent kinetic energy ($202.65 \text{ m}^2 \times \text{s}^{-2}$) and the coupling force (0.029 N) of the seeds of the B-type hole are the largest, which is the best fluid domain structure for the suction hole of the seed-metering plate, thus the corresponding knock-out wheel tooth profile was designed. Moreover, we used Adams to analyze the meshing process between the knock-out wheel and the seed-metering plate, affirming the rationality of the knock-out wheel design.

Considering the air-suction seed-metering device designed with an optimized structure as the experimental object, the response surface optimization experiment was performed based on the reasonable experimental factor level derived from the result of the one-factor experiment. With the experimental factors (seed-throwing angle, working speed, and negative pressure) and the seeding performance evaluation indicators (the qualified index, multiple index, and missing index), the influence weights of each factor on the experimental performance evaluation indicators were analyzed. The optimal combination of the experimental factors was obtained: The seed-throwing angle was 13° ; the working speed was 14.5 km/h; the negative pressure was 3.1 kPa. After verification experiments, the following corresponding experimental indicators were obtained: The qualified index was 95.9%; the multiple index was 1.2%; the missing index was 2.9%. The experimental results provide data support and a theoretical basis for the optimal design of the key structure of the air-suction vegetable seed-metering device.

Author Contributions: Conceptualization, data curation, formal analysis, investigation, methodology, software, validation, visualization, writing—original draft, and writing—review and editing, J.X.; conceptualization, data curation, methodology, resources, software, supervision, validation, visualization, and writing—review and editing, J.H.; conceptualization, data curation, formal analysis, funding acquisition, investigation, methodology, project administration, resources, supervision, validation, visualization, and writing—review and editing, W.W.; data curation, formal analysis, investigation, methodology, software, validation, visualization, and writing—original draft, C.H.; conceptualization, data curation, investigation, methodology, supervision, validation, and writing—review and editing, X.W.; data curation, investigation, methodology, software, and writing—original draft, T.T.; formal analysis, investigation, software, and validation, S.S. All authors have read and agreed to the published version of the manuscript.

Funding: This work was supported by the Key Realm R&D Program of Guangdong Province (2020B090926004, 2019B020223001) and the Agricultural Scientific Research and Agricultural Technology Extension Projects of Guangdong Province (2020-440000-02100200-8418). The authors wish to thank their generous financial assistance.

Conflicts of Interest: The authors declare no conflict of interest.

References

- Gao, X.J.; Cui, T.; Zhou, Z.Y.; Yu, Y.B.; Xu, Y.; Zhang, D.X.; Song, W. DEM study of particle motion in novel high-speed seed metering device. *Adv. Powder Technol.* **2021**, *32*, 1438–1449. [[CrossRef](#)]
- Han, D.D.; Zhang, D.X.; Jing, H.R.; Yang, L.; Cui, T.; Ding, Y.Q.; Wang, Z.D.; Wang, Y.X.; Zhang, T.L. DEM-CFD coupling simulation and optimization of an inside-filling air-blowing maize precision seed-metering device. *Comput. Electron. Agric.* **2018**, *150*, 426–438. [[CrossRef](#)]
- Jia, H.L.; Chen, Y.L.; Zhao, J.L.; Guo, M.Z.; Huang, D.Y.; Zhuang, J. Design and key parameter optimization of an agitated soybean seed metering device with horizontal seed filling. *Int. J. Agric. Biol. Eng.* **2018**, *11*, 76–87. [[CrossRef](#)]
- Ding, L.; Yang, L.; Zhang, D.X.; Cui, T.; Gao, X.J. Design and experiment of seed plate of corn air suction seed metering device based on DEM-CFD. *Trans. Chin. Soc. Agric. Mach.* **2019**, *50*, 50–60. [[CrossRef](#)]
- Yazgi, A.; Degirmencioglu, A. Optimization of the seed spacing uniformity performance of a vacuum-type precision seeder using response surface methodology. *Biosyst. Eng.* **2007**, *97*, 347–356. [[CrossRef](#)]
- Maleki, M.R.; Jafari, J.F.; Raufat, M.H.; Mouazen, A.M.; Baerdemaeker, J. Evaluation of seed distribution uniformity of a multi-flight auger as a grain drill metering device. *Biosyst. Eng.* **2006**, *94*, 535–543. [[CrossRef](#)]
- Chen, H.Y.; Liu, J.Z. Design of modular mosaic indent seed roller of rape precision seeder. *Acta Agric. Shanghai* **2010**, *26*, 96–98. [[CrossRef](#)]
- Anantachar, M.; Kumar, G.V.P.; Guruswamy, T. Development of artificial neural network models for the performance prediction of an inclined plate seed metering device. *Appl. Soft. Comput.* **2011**, *11*, 3753–3763. [[CrossRef](#)]
- Yang, W.C.; Gan, C.L.; Zhang, X.W.; Wu, Y.; Du, Q.; Pan, W.J. Design and test of precision seed metering device for panax notoginseng seedling and seeding by air suction. *Trans. Chin. Soc. Agric. Mach.* **2021**, *52*, 95–105. [[CrossRef](#)]
- Ding, L.; Yang, L.; Zhang, D.X.; Cui, T. Parametric design and test of seed cleaning mechanism of air-suction maize seed-metering device. *Trans. Chin. Soc. Agric. Mach.* **2019**, *50*, 47–56. [[CrossRef](#)]
- Lu, J.Q.; Yang, Y.; Li, Z.H.; Shang, Q.Q.; Li, J.C.; Liu, Z.Y. Design and experiment of an air-suction potato seed metering device. *Int. J. Agric. Biol. Eng.* **2016**, *9*, 33–42. [[CrossRef](#)]
- Shi, S.; Liu, H.; Wei, G.J.; Zhou, J.L.; Jian, S.C.; Zhang, R.F. Optimization and experiment of pneumatic seed metering device with guided assistant filling based on EDEM-CFD. *Trans. Chin. Soc. Agric. Mach.* **2020**, *51*, 54–66. [[CrossRef](#)]
- Yang, L.; Shi, S.; Cui, T.; Zhang, D.X.; Gao, N.N. Air-suction corn precision metering device with mechanical supporting plate to assist carrying seed. *Trans. Chin. Soc. Agric. Mach.* **2012**, *43*, 48–53. [[CrossRef](#)]
- Ding, L.; Yang, L.; Liu, S.R.; Yan, B.X.; He, X.T.; Zhang, D.X. Design of air suction high speed precision maize seed metering device with assistant seed filling plate. *Trans. Chin. Soc. Agric. Eng.* **2018**, *34*, 1–11. [[CrossRef](#)]
- Li, Z.D.; Yang, W.C.; Zhang, T.; Wang, W.W.; Zhang, S.; Chen, L.Q. Design and suction performance test of sucking-seed plate combined with groove-tooth structure on high speed precision metering device of rapeseed. *Trans. Chin. Soc. Agric. Eng.* **2019**, *35*, 12–22. [[CrossRef](#)]
- Liu, J.; Cui, T.; Zhang, D.X.; Yang, L.; Shi, S. Mechanical-pneumatic Combined Corn Precision Seed-metering Device. *Trans. Chin. Soc. Agric. Mach.* **2012**, *43*, 43–47. [[CrossRef](#)]
- Wang, F.; Lv, B.; Wang, H.M.; Zhao, M.Q. Structural design and test of seed-suction hole of air-sucking seed-metering device for millet. *Trans. Chin. Soc. Agric. Eng.* **2017**, *33*, 30–36. [[CrossRef](#)]
- Lv, J.Q.; Yang, Y.; Shang, Q.Q.; Li, Z.H.; Li, J.C.; Liu, Z.Y.; Wang, Y.B. Performance optimization test on air-suction potato seed metering device with positive pressure airflow and zero-speed seeding. *Trans. Chin. Soc. Agric. Eng.* **2016**, *32*, 40–48. [[CrossRef](#)]
- Yu, J.J.; Ding, Y.C.; Liao, Y.T.; Cong, J.L.; Liao, Q.X. High-speed photography analysis of dropping trajectory on pneumatic metering device for rapeseed. *J. Huazhong Agric. Univ.* **2014**, *33*, 103–108. [[CrossRef](#)]
- Liu, W.Z.; Zhao, M.Q.; Wang, W.M.; Zhao, S.Q. Theoretical analysis and experiments of metering performance of the pneumatic seed metering device. *Trans. Chin. Soc. Agric. Eng.* **2010**, *26*, 133–138.
- Ding, L.; Yang, L.; Zhang, D.X.; Cui, T.; Li, Y.H.; Gao, X.J. Design and test of unloading mechanism of air-suction seed metering device. *Trans. Chin. Soc. Agric. Eng.* **2020**, *51*, 37–46.
- GB/T 6973-2005; Testing Methods of Single Seed Drills. Precision Drills: Beijing, China, 2005.
- Xie, C.J.; Yang, L.; Zhang, D.X.; Cui, T.; Zhang, K.L. Seeding parameter monitoring method based on laser sensors. *Trans. Chin. Soc. Agric. Eng.* **2021**, *37*, 140–146. [[CrossRef](#)]
- He, X.T.; Hao, Y.L.; Zhao, D.Y.; Zhang, D.X.; Cui, T.; Yang, L. Design and experiment of testing instrument for maize precision seed meter's performance detection. *Trans. Chin. Soc. Agric. Eng.* **2016**, *47*, 19–27. [[CrossRef](#)]
- Guo, J.; Karkee, M.; Yang, Z.; Fu, H.; Li, J.; Jiang, Y.L.; Jiang, T.T.; Liu, E.X.; Duan, J.L. Research of simulation analysis and experimental optimization of banana de-handing device with self-adaptive profiling function. *Comput. Electron. Agric.* **2021**, *185*, 106148. [[CrossRef](#)]
- Pan, F.; Hu, B.; Luo, X.; Guo, M.; He, H. Design and Testing of a Shearing and Breaking Device for Mulch Film and Cotton Stalk Mixtures. *Trans. ASABE* **2021**, *64*, 545–555. [[CrossRef](#)]
- Shi, Y.Y.; Sun, X.; Wang, X.C.; Hu, Z.C.; Newman, D.; Ding, W.M. Numerical simulation and field tests of minimum-tillage planter with straw smashing and strip laying based on EDEM software. *Comput. Electron. Agric.* **2019**, *166*, 105021. [[CrossRef](#)]

-
28. Yang, F.Z.; Mou, J.X.; Li, W.H.; Yang, Y.P.; Li, J.D.; Yang, W. Parametric simulation design of rice precision metering tray based on Fluent/EDEM. *J. Chin. Agric. Mech.* **2020**, *41*, 1–7. [[CrossRef](#)]
 29. JB/T 10293-2013; Specifications for Single Seed Drills. Precision Drills: Beijing, China, 2013.